



Reticular liquid crystal design: Controlling complex self-assembly of *p*-terphenyl rods by side-chain engineering and chirality

Silvio Poppe^a, Anne Lehmann^a, Matthias Steimecke^a, Marko Prehm^a, Yangyang Zhao^b, Changlong Chen^b, Yu Cao^{b,*}, Feng Liu^b, Carsten Tschierske^{a,*}

^a Institute of Chemistry, Martin-Luther-University Halle-Wittenberg, Kurt-Mothes-Straße 2, 06120 Halle, Germany

^b Shaanxi International Research Center for Soft Matter, State Key Laboratory for Mechanical Behavior of Materials, Xi'an Jiaotong University, Xi'an, 710049, P. R. China

Keywords: Liquid crystal, Polyphilic self-assembly, Honeycomb phase, Rhombohedral network, Single diamond, Double gyroid, Chirality

A series of K-shaped bolapolyphiles, consisting of a *p*-terphenyl core, two polar glycerol end-groups and a swallow-tailed alkyl side-chain were synthesized and investigated. By increasing the side-chain volume an astonishing variety of very different liquid crystalline (LC) phases was observed, ranging from a rectangular ($\text{Col}_{\text{rec}}/c2mm$) and a square honeycomb ($\text{Col}_{\text{squ}}/p4mm$) via a highly complex zeolite-like octagon/pentagon honeycomb filled with additional strings of rod-bundles ($\text{Col}_{\text{rec}}^Z/c2mm$), a new 3D-hexagonal ($R\bar{3}c$) double network phase, a double and even a single network cubic phase (double gyroid $\text{Cub}/Ia\bar{3}d$ and single diamond $\text{Cub}/Fd\bar{3}m$, respectively) to a correlated lamellar phase ($\text{Lam}_{\text{sm}}/c2mm$). Though these LC structures are highly complex and there is a delicate balance of steric and geometric frustration determining the phase formation, there is only a small effect of permanent molecular chirality in the glycerol groups (*(R,R)*-configuration) on them, which is attributed to a slightly different packing density of uniformly chiral and racemic glycerols, but not to an effect of induced helicity. Compared to related T-shaped bolapolyphiles with a single linear *n*-alkyl side-chain, which form exclusively honeycomb phases, the complexity of self-assembly is enhanced for the K-shaped compounds due to a competition between the requirements of space filling, chain stretching and geometric frustration, and affected by the shape of the polar glycerol domains at the junctions.

1 Introduction

The spontaneous formation of functional structures at the nanoscale requires a combination of short-range attractive and long-range repulsive forces as well as a certain degree of dynamics

[1,2]. On the molecular level this process is important for materials chemistry and it represents an important step of abiogenesis at the transition from molecular chemistry to biological evolution [3,4]. An important state, permanently combining long range order with translational, rotational and vibrational mobility, is found in the liquid crystalline (LC) mesophases [5]. Early work on LCs lead to simple modes of organization, like nematic phases, known from display technology [6], in which the molecules have exclusively orientational long range (LR) order.

* Corresponding authors.

E-mail addresses: yu.cao@xjtu.edu.cn (Y. Cao), Carsten.tschierske@chemie.uni-halle.de (C. Tschierske).

Received 21 January 2024; Received in revised form 19 March 2024; Accepted 20 March 2024

Nevertheless, even spontaneous polar order is possible in these simple phases, leading to the recently discovered amazing ferronematic phases [7–10]. Positional order in the lamellar, columnar and cubic phases with 1D, 2D or 3D periodicity, respectively [11–15], further widens the number of phase structures and applications of LCs. They can, for example, be used as organic semiconductors [16–19], in photovoltaics [20], as light emitting diodes (OLEDs) [21] and sensors [22], offering functional structures for applications in photonics, nanotechnology and nanomedicine [23–27]. Moreover, LC research leads to insights into the basic principles of the organization of molecules at the nanoscale and provides fundamental understandings of phase transitions and the development of molecular order, polar order, uniform chirality and complexity in soft condensed matter [28–30].

Mesophases composed of self-assembled layers, columns and spheres with LR positional order are known for different soft matter systems, like aqueous micellar solutions, block copolymer morphologies and the LC phases of anisometric (e.g. rod-like or disk-like) molecules or intermolecular aggregates [31–36]. In these systems the combination of two different and mutually

incompatible types of intermolecular interactions within the molecules leads to amphiphilicity [33], i.e. to the segregation of the incompatible molecular parts into separate nano-spaces, and this is a fundamental basis of emergence of LR positional order in soft matter [37,38]. Polyphilicity, i.e. the incompatibility between more than just two incompatible units combined with the shape-anisometry is a powerful route to new complex modes of soft self-assembly if they compete with each other and generate steric and geometric frustration [28,39]. Among them, the T-shaped and X-shaped bolapolyphiles (BPs; “bola” refers to molecules with polar groups at each end of a lipophilic segment [40]) with flexible side-chains were found to assemble into complex mesophases with unique structures and properties [41–45]. The effects of rigid core length and length of linear alkyl chains has been investigated in previous work [41,42,46–48]. As shown in Fig. 1, T-shaped bolapolyphiles, consisting of a rigid *p*-terphenyl core with two terminally attached polar glycerol groups and a linear alkyl side-chain are capable of organizing into a variety of LC honeycomb phases where the end-to-end connected rod-like aromatic cores stack on top of each other and form prismatic cells of polygonal cross section shape (Fig. 1, right) [49–52]. The polar

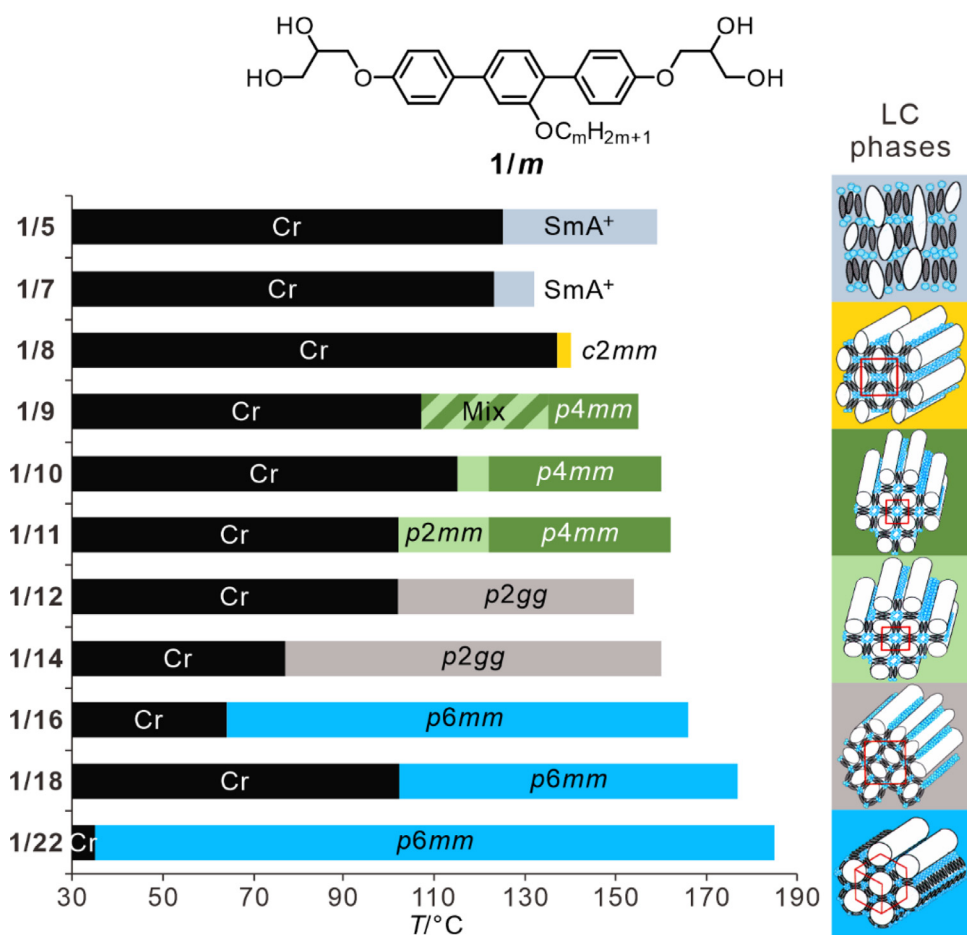
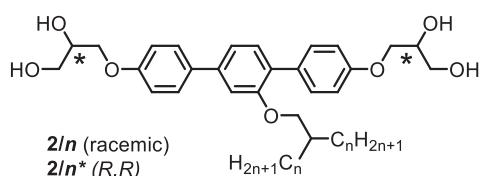


Fig. 1

Phase sequences of the T-shaped bolapolyphiles **1/m** depending on the length of the linear side-chain; at the right models of the molecular organization in the distinct mesophases (indicated by color) are shown; abbreviations: Cr = crystalline solid; SmA⁺ = distorted lamellar phase (random mesh phase); colored bars represent LC honeycomb phases formed by polygonal prismatic cells: c2mm = rhombic, p4mm = square, p2mm = rectangular, p2gg = pentagonal, and p6mm = hexagonal; the striped area of **1/9** indicates the coexistence of p4mm and p2mm; the isotropic liquid (Iso) is at the right side of the bars [49]. (For interpretation of the references to color in this figure legend, the reader is referred to the web version of this article.)

glycerol-groups, which organize in extended intermolecular hydrogen bonding networks [53] segregate from the polyaromatic cores and form columns (blue) along the *c*-direction, thus connecting the rod-like cores at the edges, and leading to honeycomb frameworks, while the flexible side-chains fill the interior of the resulting polygonal prismatic cells.

Even longer chains can lead to honeycombs composed of giant polygons and to lamellar (Lam) phases [48,54–56]. It was also shown that branching the side-chains provides new types of cubic network phases composed of coaxial bundles of the rods interconnected by glycerol spheres as junctions and having different junction geometries [57–64]. This design concept was expanded to facial polyphiles with alkyl chains forming the junctions [65], and recently to giant sphere-rod conjugates [66]. Moreover, this chemistry based molecular design work is accompanied by simulation work from several groups [67–75]. Among the reported structures, the K-shaped bolapolyphilic *p*-terphenyls with a branched side-chain (compounds **2/n**) arose special interest. In previous communications the formation of a new complex pentagon-octagon tiling pattern [76] and the first example of a single network cubic phase with 4-way junctions, the single diamond (SD) phase, were discovered for this kind of compounds [61].



However, all bolapolyphiles with two glycerol end-groups involve two stereogenic centres with either (*R*)- or (*S*)-

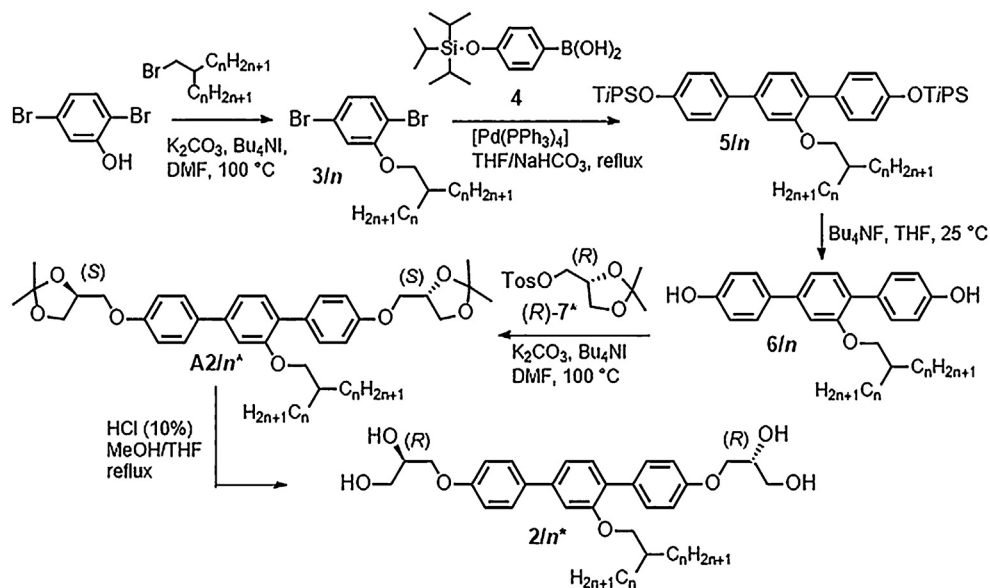
configuration (indicated by asterisks), thus representing mixtures of four stereoisomers (in the following abbreviated as “racemic mixtures” or “racemates”). In all previously reported cases the compounds were synthesized as such racemic mixtures of (*R,S*)/(*S,R*)- and (*R,R*)/(*S,S*)-diastereomers. It is known that stereochemical purity can induce new structures in lyotropic and thermotropic mesophases of amphiphilic [77] as well as rod-like molecules [78].

Thus, the purpose of this work is twofold. Firstly, bolapolyphiles with uniform (*R,R*)-configuration of their stereogenic centres were synthesized for the first time and the self-assembly of these enantiomeric pure compounds is compared with that of the corresponding “racemic” mixtures. Secondly, the series of racemic compounds was completed and the previously not considered low temperature LC phases of compounds **2/n** were investigated and their structures determined. Thus, the full sequence of complex nanostructures evolving for K-shaped molecules at the transition from honeycombs via a combination of honeycombs with columns to interwoven double and even single networks of branched columns is uncovered. This also leads to the discovery of a new double network LC phase with hexagonal symmetry based on a gyroid-like interface. Finally, the differences between the self-assembly of molecules with linear and branched side-chains will be worked out and explained, providing general rules for tailoring of complex soft matter nanoscale structures based on side-chain engineering.

2 Methods

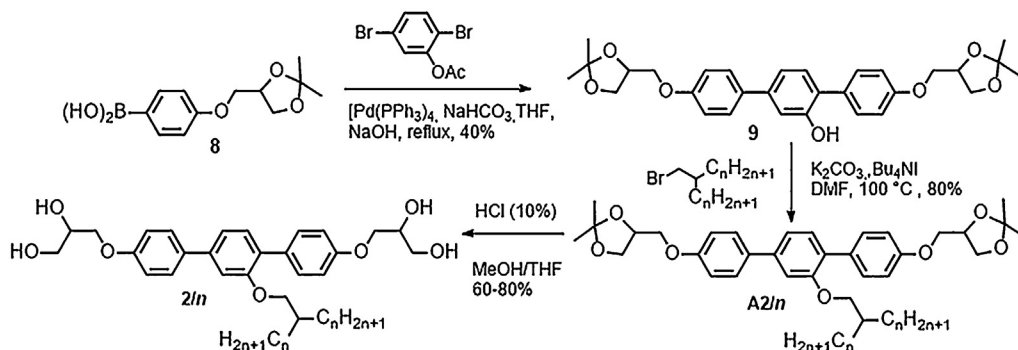
2.1 Materials

As shown in Scheme 1, the synthesis of compounds **2/n*** with (*R*)-configuration of the glycerol units starts with the alkylation of 2,5-dibromophenol [79] with 1-bromo-2-alkylalkanes [52], yielding the dibromophenylethers **3/n**, which were then coupled



Scheme 1

Synthesis of the compounds **2/n***; note that the absolute configuration of the stereogenic centers in (*R*)-**7***, (*S,S*)-**A2/n*** and (*R,R*)-**2/n*** remains the same though the stereochemical descriptors change.



Scheme 2

Synthesis of the “racemic” compounds **2/n**.

with 4-(triisopropylsilyloxy)phenylboronic acid (**4**) [80] in a Suzuki cross coupling reaction to the corresponding 4,4'-bis(triisopropylsilyloxy)-*p*-terphenyls **5/n**. After desilylation with Bu_4NF [81], the obtained 2'-substituted *p*-terphenyl-4,4'-diols **6/n** were alkylated with two equivalents of (*R*)-2,2-dimethyl-1,3-dioxolane-4-methanol-*p*-toluenesulfonate ((*R*)-**7***, $[\alpha]_D - 4.9^\circ$, $c = 1 \text{ mol/L}$ in EtOH, >99% ee, Aldrich) to give the acetonides **A2/n***. The following deprotection with diluted HCl in MeOH/THF yielded the desired (*R,R*)-compounds **2/n***. During the reactions the stereogenic center of (*R*)-**7*** was not touched and therefore the enantiomeric purity of compounds **2/n*** should correspond to that of the employed (*R*)-**7***.

The synthesis of the “racemates” **2/n** with even numbers $n = 10\text{--}22$ has been reported previously [61,76]. All new “racemic” compounds **2/n**, i.e. those with $n < 10$ and those with odd numbered n were synthesized in an analogous way by alkylation of “racemic” 4,4'-bis(2,2-dimethyl-1,3-dioxolane-4-yl-methoxy)-*p*-terphenyl-2-ol (**9**) [76] with appropriate branched 1-bromo-2-alkylalkanes, followed by deprotection of the glycerol end groups (see Scheme 2) [52]. The procedures and analytical data of compounds **2/n*** and all new compounds **2/n** are collated in Section S5 of the Supplementary Materials.

2.2 Techniques

All compounds were heated for 3 min to the isotropic liquid state (at least to 140 °C) prior to investigation to remove all water traces adsorbed by the glycerol units, and were immediately covered or sealed.

Polarizing optical microscopy (POM) was conducted with a Leica DMR XP polarizing microscope in conjunction with a heating stage (FP 82 HT, Mettler) and controller (FP 90, Mettler). Optical investigation was carried out under equilibrium conditions between glass slides which were used without further treatment, sample thickness was $\sim 15 \mu\text{m}$. A full wavelength retardation plate was used to determine the sign of birefringence. Optical micrographs were taken using a Leica MC120HD camera; see Sections S1.2 and S2.2 in the Supplementary Materials for representative textures.

Differential scanning calorimetry (DSC) scans were performed with a DSC-7, Perkin Elmer in sealed aluminum pans (30 μL) under dry N_2 at heating/cooling rates of 10 K min^{-1} ; peak

temperatures are given in the Tables 1 and 2: for DSC traces, see Figs. S1, S2 in the Supplementary Materials.

In-house small-angle and wide-angle X-ray scattering (SAXS and WAXS) was carried out using Ni filtered $\text{CuK}\alpha$ radiation (Kristalloflex 760H, Siemens, 15 to 30 min exposure time). Aligned samples were obtained on a glass plate. Alignment was achieved upon slow cooling (rate: $1 \text{ K min}^{-1} - 0.01 \text{ K min}^{-1}$) of a small droplet of the sample. The aligned samples were held on a temperature-controlled heating stage and the diffraction patterns were recorded with a 2D detector (Vantec 500, Bruker). The sample-detector distance for the samples was 9.00 cm for WAXS and 26.70 cm for SAXS measurements.

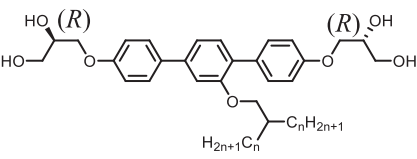
Synchrotron small-angle X-ray scattering experiments were conducted at beamline BL16B1 at Shanghai Synchrotron Radiation Facility (SSRF). For powder SAXS the samples were filled into evacuated 1 mm diameter capillaries. A modified Linkam hot stage and a Pilatus 2M CCD are used in SSRF. Heating and cooling process were conducted with a rate of 10 K min^{-1} , in line with DSC. Data calibration was conducted by a series of *n*-alkanes and silver-borohydride (AgB). The transformation of 2D data to 1D plot is carried out by Irena and Nika macro on Igor64 platform with Gauss equation. With proper indexing from space group and integrated peak intensities, the 2D&3D electron density ($\rho(x, y)$ & $\rho(x, y, z)$) maps were reconstruct via Fourier transform (FT) as:

$$\rho(x, y) = \sum_{hk} \sqrt{I(hk)} \exp [2\pi i(hx + ky) + i\phi_{hk}]$$

$$\rho(x, y, z) = \sum_{hkl} \sqrt{I(hkl)} \exp [2\pi i(hx + ky + lz) + i\phi_{hkl}]$$

For centrosymmetric structures with the electron density $\rho(x, y, z) = \rho(\bar{x}, \bar{y}, \bar{z})$, the phase ϕ_{hkl} is either 0 or π . This allows an exhaustive approach by comparing all possible phase combinations. The best combination is determined by physical merit of reconstructed electron density (ED) map and other information from the system, like volume ratio of aromatic/aliphatic region and ED distribution histogram. This method works well for LC system with only few intense peaks. For details, see Sections S1.3 and S2.3 in the Supplementary Materials.

Table 1

Data of the enantiomers **2/n*** with (*R*)-configuration of both stereogenic centers.^a


Compd.	<i>T</i> /°C, [ΔH]/kJ·mol ⁻¹	<i>a</i> , <i>b</i> /nm (<i>T</i> /°C)	<i>n</i> _{cell}	<i>n</i> _{wall} / <i>n</i> _{bundle}
2/10*	Cr 82 [8.1] Col _{rec} ^Z / <i>c2mm</i> 146 [4.4] Iso	15.92, 6.34 (100)	37.6 ^b	1.9/9 ^b
2/12*	H: Cr 76 [29.8] Col _{rec} ^Z / <i>c2mm</i> 118 [2.6] Cub/ <i>la3d</i> 143 [1.4] Iso	16.04, 6.32 (80)	34.5 ^b	1.7/9 ^b
	C: Iso 135 [1.1] Cub/ <i>la3d</i> 107 [1.1] Hex/ <i>R3c</i> 100–93 [1.2]	7.72 (122)	348 ^c	15 ^c
	Col _{rec} ^Z / <i>c2mm</i> 45 [5.4] Cr	10.65, 7.53	526 ^d	15 ^d
		(106, cooling)		
2/14*	Cr 104 [30.8] Lam _{sm} / <i>c2mm</i> 108 [2.4] Cub/ <i>la3d</i> 161 [2.2] Iso	7.71 (136)	320 ^c	13 ^c
		5.89, 2.20 (62)	4.1 ^e	2.1 ^e
2/16*	Cr 79 [19.5] Lam _{sm} / <i>c2mm</i> 114 [4.2] Cub/ <i>la3d</i> 161 [2.1] Iso	7.69 (130)	294 ^c	12 ^c
		6.18, 2.22 (80)	4.0 ^e	2.0 ^e
2/18*	Cr 65 [49.6] Lam _{sm} / <i>c2mm</i> 104 [4.1] Cub/ <i>Fd3m</i> 131 [0.8]	6.53, 2.22 (75)	3.9 ^e	2.0 ^e
	Cub/ <i>la3d</i> 143 [0.7] Iso	6.41 (100)	159 ^f	10 ^f
		7.65 (135)	270 ^c	11 ^c
2/20*	Cr 51 [32.7] Cub/ <i>Fd3m</i> 166 [2.8] Iso	6.45 (100)	151 ^f	9 ^f

^a Transition temperatures were taken from the second DSC heating scan (10 K·min⁻¹, peak temperature, see Figure S1); phase sequences on 2nd cooling are only shown for cases with different phase sequences on heating (H) and cooling (C); for all other compounds the transitions on cooling are listed in Table S1; the highest observed melting point and the total of all Cr-Cr transition and melting enthalpies are shown; Abbreviation: Col_{rec}^Z/*c2mm* = giant rectangular honeycomb LC phase combining pentagonal and filled octagonal cells (Fig. 2h); Lam_{sm}/*c2mm* = lamellar phase with AB correlated layers; Cub/*la3d* = unicontinuous cubic network phase with segmented double gyroid structure (DG), Hex/*R3c* = unicontinuous hexagonal network phase with distorted double gyroid structure; Cub/*Fd3m* = unicontinuous cubic network phase with segmented single diamond network (SD) structure; the crystallographic space groups are shown after the slash; *n*_{cell} = number of molecules in one unit cell; *n*_{wall} = number of molecules in the lateral cross section of the individual honeycomb walls dividing the prismatic cells; *n*_{bundle} = number of molecules forming one molecular bundle; for DSCs, see Figs. 2a, 6a and S1.

^b Values of Col_{rec}^Z/*c2mm* (see Section S4.2 for estimation of the *n*_{wall}/*n*_{bundle} values, note that each molecule organized in the rod-bundles contributes to the space filling in a stack of approximately 5 unit cells, 0.45 nm per cell).

^c Cub/*la3d*.

^d Hex/*R3c*.

^e Lam_{sm}/*c2mm*.

^f Cub/*Fd3m* phase.

3 Results and discussion

The phase sequences and transition temperatures of the (*R,R*)-enantiomers **2/n*** and the racemic mixtures of diastereomers **2/n**, are collected in Tables 1 and 2, respectively.

3.1 Homochiral compounds **2/n***

In this section the LC phases of the (*R,R*)-enantiomers **2/10***–**2/20*** (Table 1) with even numbered *n* will be analysed and compared with the related phases of the racemic mixtures **2/10**–**2/20** (Table 2), while in the next section the focus will be on compounds with shorter chains and the effects of chain branching in comparison to linear chains.

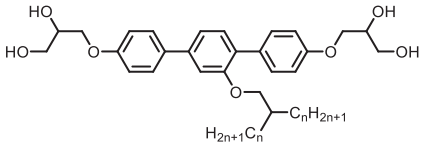
3.1.1 Zeolite like pentagon-octagon tessellation with filled octagons (Col_{rec}^Z/*c2mm*)

For compound **2/10*** and **2/12*** a biaxial birefringent mesophase with *c2mm* plane group and large lattice was found as the first mesophase formed upon melting the crystalline samples. As representative example, compound **2/12*** is described here in more detail (Fig. 2). The SAXS pattern is indexed to a rectangular lattice with large lattice parameters of *a*_{rec} = 16.04 nm (~7 *L*_{mol}) and *b*_{rec} = 6.32 nm (~3 *L*_{mol}; *L*_{mol} = molecular length between the ends of the glycerol groups = 2.1–2.6 nm, see Fig. S25a) at 80 °C, indicating the formation of a complex superlattice structure (Fig. 2c, Tables S2, S3). The diffuse WAXS with a maximum at

d = 0.45 nm (Figs. 2c, d and S5) and the fluidity of the sample upon shearing confirms the LC character of this mesophase with 2D lattice. It shows a spherulitic texture with large domains and negative birefringence (Figs. 2g), typical for a columnar phase with an alignment of the π -conjugated *p*-terphenyl rods predominately in the lattice plane (*a/b* plane) and perpendicular to the column main axis (*c* direction), in line with a honeycomb LC phase.

The ED map, reconstructed from the diffraction pattern of **2/12*** (Fig. 2c) is displayed in Fig. 2e. It shows a high ED network (purple-blue-green) involving the *p*-terphenyl cores and glycerol end-groups separating cells filled by the low ED alkyl chains (red-yellow-green) with the larger cells containing additional high ED ellipses. Considering the molecular dimensions, the ED map of **2/12*** can be interpreted as composed of pentagonal prismatic cells arranged in parallel ribbons where adjacent pentagons assume an antiparallel orientation, and the pentagonal prismatic cells are filled by the alkyl side-chains (Fig. 2e, h). These ribbons of pentagons are interconnected at the apexes of the pentagons to form octagonal cells between them. The excess space in these giant octagonal cells is filled by additional columns of end-to-end connected bundles of coaxial aligned molecules [82], leading to the additional ED maxima (blue/purple) in the middle of the octagonal cells. This LC structure, corresponding to that reported for racemic **2/10** [76], combines two different types of rod-orientations. The majority of *p*-terphenyls forming the

Table 2

Phase transitions and structural data of the racemic mixtures of diastereomers **2/n**.^a


Compd.	$T/^\circ\text{C}$, [$\Delta H/\text{kJ}\cdot\text{mol}^{-1}$]	$a, b/\text{nm}$ ($T/^\circ\text{C}$)	n_{cell}	$n_{\text{wall}}/n_{\text{bundle}}$
2/4	Cr 131 [7.2] Col _{rec} /p2mm 141 [0.49] Col _{squ} /p4mm 158 [3.7] Iso	2.63 (150)	3.6 ^b	1.8 ^b
		3.03, 2.38 (135)	3.8 ^c	1.9 ^c
2/6	Cr 95 [3.7] Col _{rec} /p2mm 107 [0.6] Col _{squ} /p4mm 175 [7.3] Iso	2.64 (160)	3.2 ^b	1.6 ^b
		3.09, 2.37 (105)	3.4 ^c	1.7 ^c
2/8	Cr 128 [25.3] Col _{squ} /p4mm 157 [4.2] Iso	2.64 (150)	2.8 ^b	1.4 ^b
2/9	Cr 120 [19.5] Col _{rec} ^Z /c2mm 148 [4.3] Iso	15.82, 6.35 (135)	39.5 ^d	n.d. ^k
2/10 [61]	Cr 75 [7.1] Col _{rec} ^Z /c2mm 147 [4.5] Iso	15.94, 6.24 (140)	37.0 ^d	1.9/9 ^d
2/11	Cr 97 [23.2] Col _{rec} ^Z /c2mm 139 [4.3] Iso	15.94, 6.37 (125)	36.4 ^d	n.d. ^k
2/12 ⁱ [61]	H: Cr 79 [18.8] Col _{rec} ^Z /c2mm 120 [2.7] Cub/la3d 148 [1.6] Iso	16.01, 6.32 (80)	33.6 ^d	1.7/9 ^d
	C: Iso 142 [1.2] Cub/la3d 111 [1.0] Hex/R3c 102–85 [1.4]	7.76 (120)	354 ^e	15 ^e
	Col _{rec} ^Z /c2mm 48 [5.9] Cr	10.65, 7.68 (108, cooling)	537 ^f	15 ^f
2/13	Cr 102 [36.7] Lam _{sm} /c2mm 109 [3.3] Cub/la3d 158 [1.9] Iso	5.63, 2.19 (90)	4.0 ^g	2.0 ^g
		7.76 (120)	339 ^e	14 ^e
2/14 ⁱ [61]	Cr 104 [30.8] Lam _{sm} /c2mm 108 [2.2] Cub/la3d 161 [2.3] Iso	5.80, 2.20 (90)	4.0 ^g	2.0 ^g
		7.71 (130)	320 ^e	13 ^e
2/15	Cr 86 [27.0] Lam _{sm} /c2mm 112 [4.0] Cub/la3d 162 [2.3] Iso	5.96, 2.21 (90)	4.0 ^g	2.0 ^g
		7.62 (140)	297 ^e	12 ^e
2/16 ⁱ [61]	Cr 78 [18.6] Lam _{sm} /c2mm 114 [4.0] Cub/la3d 160 [2.1] Iso	6.04, 2.19 (90)	3.9 ^g	1.9 ^g
		7.71 (120)	297 ^e	12 ^e
2/18 ⁱ [61]	Cr 62 [65.5] Lam _{sm} /c2mm 103 [5.0] Cub/Fd3m 134 [0.8]	6.52, 2.21 (70)	3.9 ^g	2.0 ^g
	Cub/la3d 139 [0.8] Iso	6.39 (110)	157 ^h	10 ^h
		7.59 (135)	264 ^e	11 ^e
2/20 [61]	Cr 71 [74.2] Cub/Fd3m 168 [2.7] Iso	6.32 (150)	143 ^h	9 ^h
2/22 [61]	61 [51.7] Cub/Fd3m 172 [3.9] Iso	6.32 (160)	134 ^h	8 ^h

^a Data were taken from the second DSC heating scans (10 K·min⁻¹, peak temperatures); phase sequences on 2nd cooling are only shown for cases with different phase sequences on heating (H) and cooling (C); for all other compounds the transitions on cooling are listed in Table S11; only the highest melting point and the total of all Cr-Cr transition- and melting-enthalpies are shown. The DSCs of all new compounds are shown in Fig. S10a-g. Abbreviation: Col_{rec}/p2mm = rectangular honeycomb, Col_{squ}/p4mm = square honeycomb, for other abbreviations, see Table 1.

^b Values of Col_{squ}/p4mm.

^c Col_{rec}/p2mm.

^d Col_{rec}^Z/c2mm (see comments in Table 1).

^e Cub/la3d.

^f Hex/R3c.

^g Lam_{sm}.

^h Cub/Fd3m.

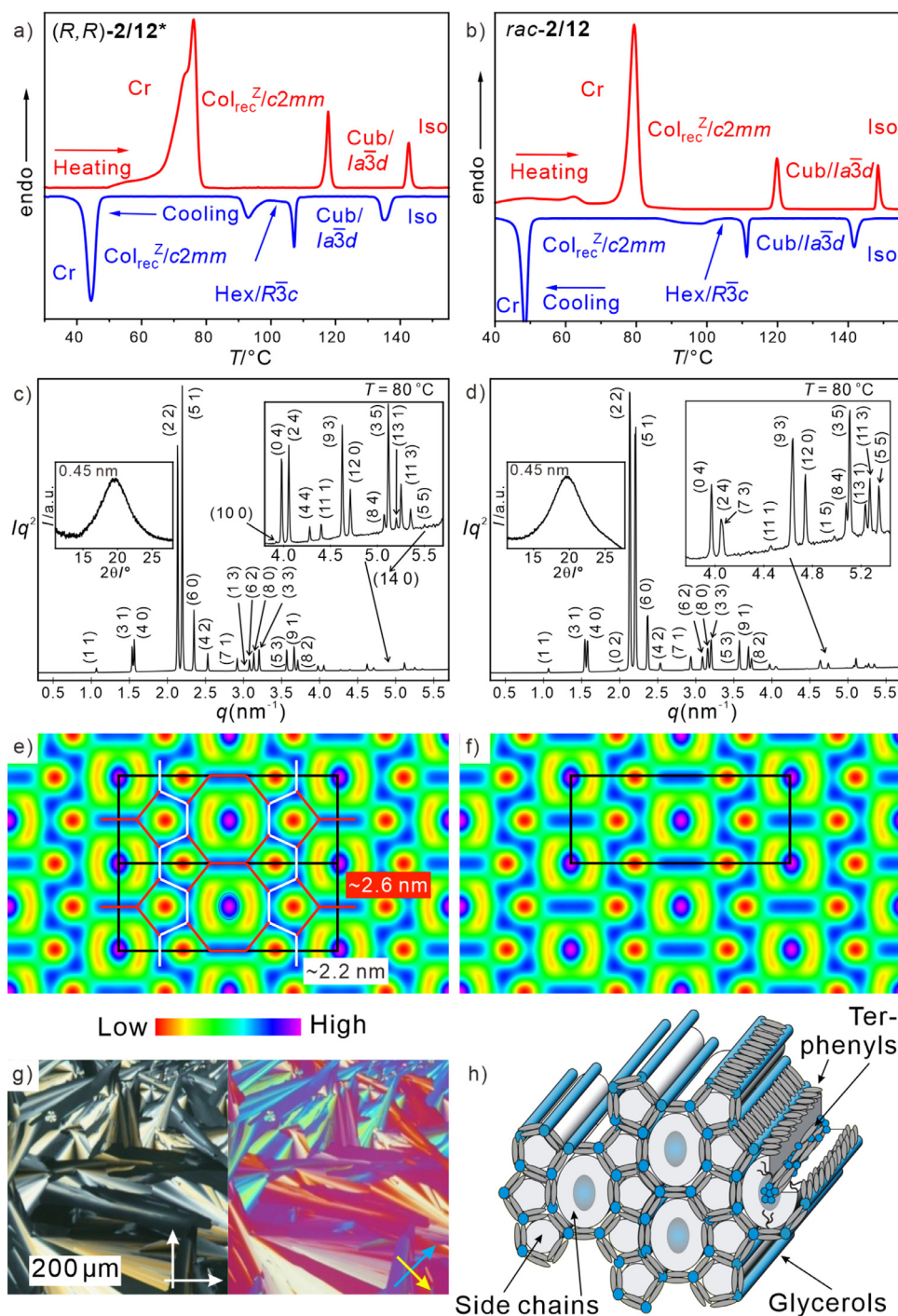
ⁱ Focus of the previous report was only on the SD and DG phases while the low temperature phases (Lam_{sm}/c2mm, Col_{rec}^Z/c2mm and Hex/R3c) were not investigated, for **2/18** an additional Fd3m-la3d transition was detected which was previously not recognized [61]; the data of these compounds were revised accordingly.

^j Reinvestigation of **2/20** [61] indicated a crystalline modification with higher m.p. than previously reported (see Fig. 10h).

^k Not determined because no ED maps were available.

honeycomb network are arranged in the *a-b* plane, where each honeycomb wall contains about 2 molecules in the cross section ($n_{\text{wall}} = 1.7\text{--}1.9$, see Table 1), in line with other honeycomb phases of compounds with a single side-chain. The remaining *p*-terphenyls form the rod-bundle columns, which are organized in the perpendicular direction, i.e. parallel to the *c*-direction (Fig. 2h). Similar to Col_{hex} phases formed by columns of end-to-end connected rod-bundles on a hexagonal lattice [82], each column involves about 9 molecules (n_{bundle} , see Section S4.2 for estimation of these values). Because the number of molecules in the honeycombs exceeds that in the rod-bundle columns (~31:3.6), negative birefringence is retained, but slightly reduced if compared with simple honeycombs [76]. This unique LC structure results from the competition between side-chain volume and side-

chain length. The side-chain volume would require hexagonal honeycombs, as observed for the related T-shaped compound **1/22** (see Fig. 1) [49], with approximately the same side-chain volume ($m = 2n+2$ CH₂ units). However, as measured for the *p6mm* phase of **1/22**, the minimum requirement of alkyl chain length is ~2.1 nm, exceeding the *all-trans* alkyl chain length of **2/12*** (distance between the terphenyl rod and the ends of the branches = 14 carbons ~1.9 nm, see Fig. S26d). Thus, the pentagon is the largest possible polygon for which the side-chains can bridge the gap between the aromatic walls and the centres of the polygons without significant chain stretching, which would be entropically disfavoured. Because the chain volume exceeds the available space in the pentagons, some of the side-chains are forced to escape from these pentagons. This

**Fig. 2**

$\text{Col}_{\text{rec}}^Z/c2mm$ phase. a, b) DSC heating and cooling traces at a rate of 10 K min^{-1} a) of the (R,R) -enantiomer $2/12^*$, b) of racemic $2/12$, and c, d) SAXS diffractograms of c) (R,R) -enantiomer $2/12^*$ and d) racemic $2/12$ at 80°C upon cooling; insets: WAXS diffractograms with diffuse scattering maximum at 0.45 nm , indicating the liquid crystallinity; e, f) ED maps calculated by the first 6 reflexes (phase combination: $\pi\pi 0000$, for ED maps using 12 scattering peaks, see Fig. S18). The lattice is indicated by black lines and p -terphenyl cores are arranged along the white and red lines; g) texture of (R,R) -enantiomer $2/10^*$ between crossed polarizers (left) and with additional full wave plate (right) at $T = 145^\circ\text{C}$; h) shows a perspective model of the honeycomb structure; for NMR spectra of rac- $2/12$ and (R,R) - $2/12^*$, see Figs. S30-S33. (For interpretation of the references to color in this figure legend, the reader is referred to the web version of this article.)

inhibits the development of a uniform pentagonal honeycomb and allows only the formation of ribbons with antiparallel arranged pentagonal prismatic cells. Neighbouring ribbons are interconnected by additional molecules via the pentagon-apexes

with formation of octagonal cells between them (Fig. 2e, f). At the outside edges of the pentagon-ribbons the excess alkyl chains, not fitting into the pentagons, contribute to the filling of the much larger octagons. Again, the branched lateral chains are much too

short to fill the interior of these octagons, leaving large voids. These voids provide sufficient space to accommodate additional columns formed by the end-to-end connected coaxial rod-bundles with their side-chains.

In the honeycombs there are edges of two different lengths. The shorter ones (along the white lines in Fig. 2e, connecting three sides of each pentagon) is ~ 2.2 nm, correspond to the minimal molecular length ($L_{\text{mol}} = 2.1$ nm, Fig. S25a) as measured between the secondary OH groups of the glycerols in a compact conformation. The longer ones (red segments in Fig. 2e), separating the octagons and the pentagons from the octagons are ~ 2.6 nm, corresponding to the length of the rod-like core between the primary OH groups at the ends of the glycerol groups in the most extended conformation. ($L_{\text{mol}} = 2.6$ nm, Fig. S25a). For comparison, the side length in the hexagonal honeycomb of **1/22** with linear side-chain is 2.43 nm [49], being in the middle between these two values. The shrinkage of the three neighbouring pentagon walls is attributed to the limited chain length, favouring reduction of the pentagon size to be able to reach their centres at minimal entropy loss by chain stretching. On the other hand, the pentagons are still too small to accommodate the large chain volume (requiring hexagons). This requires expansion of some pentagon walls to a length of 2.6 nm which appears to be easier for those forming the apexes (located on the red lines). Moreover, the majority of molecules forming the apexes of the pentagons give their side-chains into the octagons. This leads to a looser packing of the aromatics in these walls (due to collisions of the bulky side-chains at the same side), thus having a lower ED (green) compared to the others. There is obviously no communication between the rod-bundle columns in the octagonal cells and thus no correlation of the periodicities along neighbouring columns of coaxial rod-bundles. Therefore, there is only 2D periodicity and no indication of any additional periodicity along the *c*-direction can be observed [82]. This unique LC phase combines different signs of the curvature of the inter-material dividing surfaces (IMDS) between the polar and rigid bolaamphiphilic cores and the flexible and lipophilic side-chains, being negative for the rod-bundle columns and positive for the surrounding honeycomb. Moreover, this 2D tiling pattern composed of pentagons and octagons resembles the projection of the BIK-type [83] zeolites (okenite [84] and bikitaite [85]) if viewed along their (001) axis and therefore this LC phase was designated as $\text{Col}_{\text{rec}}^{\text{Z}}/c2mm$, where the superscript Z indicates the zeolite-like super-lattice structure of this honeycomb LC phase [76]. Even the incorporation of additional molecules in the voids of the large octagonal cells is similar to the capability of zeolitic solid state frameworks to incorporate guest molecules. Interestingly, a similar structure combining strings of antiparallel pentagonal cells, but with hexagonal instead of the octagonal cells and without additional columns filling the larger cells, has recently been reported for a block copolymer morphology [86].

The diffraction pattern and the lattice parameters of the $\text{Col}_{\text{rec}}^{\text{Z}}/c2mm$ phases of the enantiomer **2/12*** correspond to those of **2/10*** and the racemic mixtures **2/12** & **2/10** [76] with only minimal deviations (see Fig. 2c, d and Tables 1, 2). This means that there is no visible difference in the ED maps (Fig. 2e, f) or difference in molecular self-assembly between pure enantiomer

and racemate, and also no indication of any macroscopic helical superstructure can be found. Small differences of some scattering intensities were observed for the $\text{Col}_{\text{rec}}^{\text{Z}}/c2mm$ phases of **2/12** and **2/12*** (Fig. 2c, d), which however have no visible influence on the ED maps. These differences are not consistent features of enantiomers/racemates and for example are inverted for the pair **2/10** [76] & **2/10***. Though the origin of these small differences is not yet clear, we attribute it more to differences in packing densities than to specific chirality effects. For **2/10*** and the racemates **2/9-2/11** the $\text{Col}_{\text{rec}}^{\text{Z}}/c2mm$ phase is the only LC phase, while for **2/12*** it is accompanied at higher temperature by cubic and non-cubic network phases ($R\bar{3}c$, $Ia\bar{3}d$, see next Sections 3.1.2 and 3.1.3), and for **2/14*** the $\text{Col}_{\text{rec}}^{\text{Z}}/c2mm$ phase is completely replaced by a lamellar phase at low temperature ($\text{Lam}_{\text{Sm}}/c2mm$), while the cubic network phase at higher temperature is retained (Tables 1 and 2).

3.1.2 Double gyroid network phase ($DG = \text{Cub}/Ia\bar{3}d$)

On heating **2/12*** the birefringent $\text{Col}_{\text{rec}}^{\text{Z}}/c2mm$ phase is at $T = 118$ °C replaced by an optically isotropic phase with high viscosity, as typically observed for cubic phases. For this compound and the longer homologues **2/14*** and **2/16*** the *q*-values of the SAXS patterns in this isotropic mesophase show a characteristic ratio of $\sqrt{6}:\sqrt{8}:\sqrt{14}:\sqrt{16}:\sqrt{20}:\sqrt{22}$, which was indexed as (211), (220), (321), (400), (420) and (332) reflections of a cubic $Ia\bar{3}d$ lattice with lattice parameters around 7.7 nm ($\sim 3 \times L_{\text{mol}}$), remaining almost constant for all compounds **2/12*-2/16*** (Figs. 3, S6-S8 and Tables S8, S10 and ref. [61]). The diffuse scattering at $d = 0.46$ nm (Fig. 3a, c) confirms the LC state. The diffraction pattern and the reconstructed ED map of the cubic phase of the enantiomer **2/12*** are shown as typical examples in Fig. 3a, b. The $Ia\bar{3}d$ lattice is formed by a double gyroid (DG) network with the rods arranged in coaxial bundles forming two interwoven networks with three-way junctions interconnecting these bundles (Fig. 3d, e). There is a uniform twist of 70.5° between adjacent junctions and this leads to two interpenetrating enantiomeric chiral networks (indicated by red and blue spheres, respectively) which are separated by the gyroid (G) periodic infinite minimal surface. Similar to the *meso*-diastereomers of molecules combining two enantiomeric stereogenic centres the two networks are inseparably connected, and thus this double Gyroid (DG) phase can be considered as an achiral supramolecular *meso*-structure [87].

In the ED map the networks with high ED (green, blue, purple) involve the struts formed by bundles of terphenyl cores and the glycerols domains forming the junctions, while the continuum with low ED (not shown for clarity) is filled by the disordered alkyl side-chains (Fig. 3b, d, e). The distance between the network junctions (d_{nodes}), calculated to $d_{\text{nodes}} = a_{\text{cub}}/(2 \cdot \sqrt{2}) = 2.7$ nm [58] is close to the maximum molecular length between the two primary OH groups, assuming the most stretched conformation of the glycerol groups ($L_{\text{mol}} = 2.6$ nm, Fig. S25a). The minor deviation could be attributed to the deformation of the nodes formed by the hydrogen bonded glycerol domains by assuming a triangular shape (Fig. S28a). Accordingly, the *p*-terphenyl units arrange in coaxial bundles (struts) which are connected with each other by the polar hydrogen bonded domains of the nano-segregated

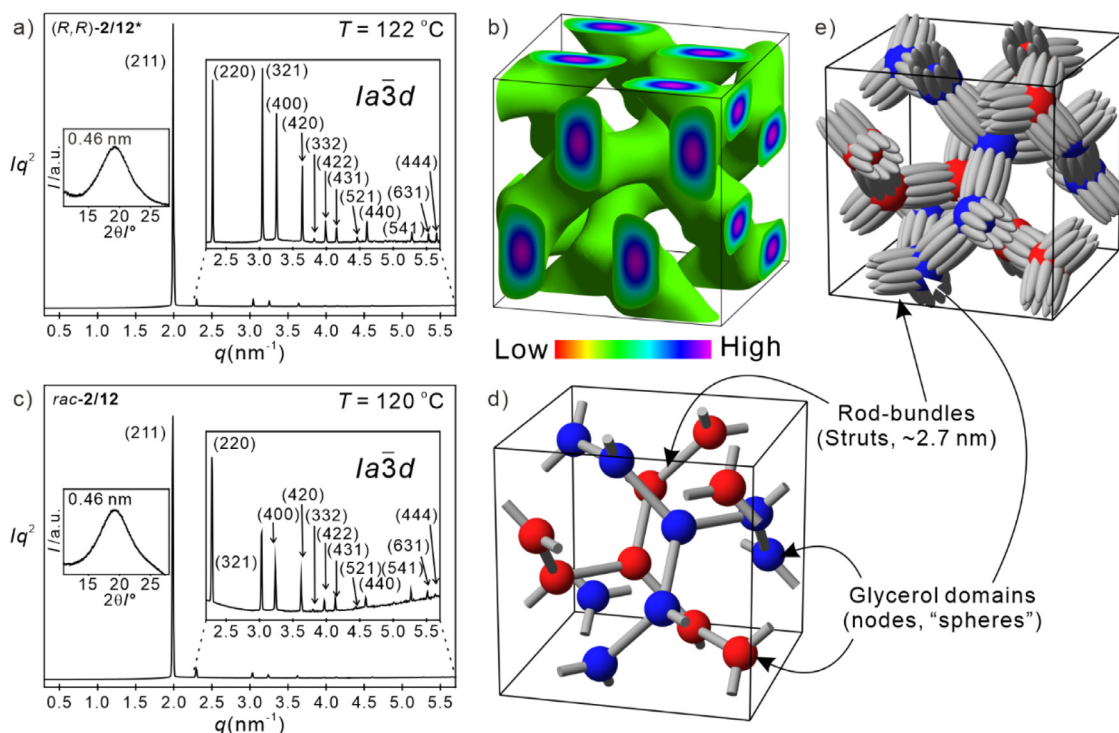


Fig. 3

a, b) SAXS pattern of the *(R,R)*-enantiomer **2/12*** at 122 °C and ED map reconstructed from the diffraction pattern; c) SAXS pattern of racemic **2/12** at 120 °C, insets: WAXS diffractograms with diffuse scattering with maximum at 0.46 nm; d) stick-and-ball model showing the double network structure of the $Ia\bar{3}d$ phase; red and blue nodes indicate the networks with opposite handedness; though the glycerol domains are shown as spheres they are actually deformed to truncated triangles; e) shows a model with the coaxial *p*-terphenyl bundles interconnecting the nodes. (For interpretation of the references to color in this figure legend, the reader is referred to the web version of this article.)

glycerols forming three-way junctions. Thus, only the side-chains form a continuum around the networks, while the networks themselves are not continuous. This DG phase with segmented networks is considered as an uncontinuous double network phase to distinguish it from the bicontinuous network phases having non-segmented continuous networks (for further explanations, see ref. [58], especially Fig. 2 and related text in this reference). The nano-segregated glycerol domains at the junctions could be considered as “mesoatoms” [88,89] with coordination number of $CN = 3$ and the bundles of *p*-terphenyls acting as “bonds” between them. Despite of side-chain expansion with growing chain length the cubic lattice parameter is around $a_{\text{cub}} = 7.7$ nm for all compounds **2/12***–**2/18*** (Table 1). This is due to the fixed length of these “bonds” and becomes possible by reduction of the number of molecules arranged in the lateral cross section of the rod-bundles with growing side-chain volume from $n_{\text{bundle}} \sim 15$ for **2/12*** to ~ 11 for **2/18***. Such large n_{bundle} numbers, exceeding 5–7, require a partial mixing between alkyl chains and aromatic core in the periphery of the struts, in line with the lower ED shell in green around the high ED (blue/purple) cores (Fig. 3b).

The DG can be observed for all enantiomers **2/12*** – **2/18*** as well as for their racemic mixtures **2/12** – **2/18** [61] and the lattice parameters found for racemates and enantiomers are almost identical (compare Tables 1 and 2, maximal deviation is 0.1 nm). This means that the diastereomeric relations between molecular

chirality and network chirality appear to have no measurable effect on their LC self-assembly in the DG networks.

3.1.3 3D-hexagonal network phase ($Hex/R\bar{3}c$)

Investigation of **2/12*** revealed an additional mesophase occurring between $Col_{\text{rec}}^Z/c2mm$ and DG on cooling. While there is only one direct transition with a sharp DSC peak from the $Col_{\text{rec}}^Z/c2mm$ phase to the DG on heating, on cooling from the DG phase the $Col_{\text{rec}}^Z/c2mm$ phase is not directly formed, but in a two-step process with an additional intermediate phase (Figs. 2a, 4a, c and Tables 1, 2, S4, S5). For **2/12*** at the first transition from the DG phase at 107 °C a low birefringent striped texture composed of small mosaics (Fig. 4a, inset) develops which is slowly replaced by the well-developed spherulitic texture of the $Col_{\text{rec}}^Z/c2mm$ phase taking place in the temperature range around 100–93 °C (Figs. 2a and S2). The SAXS pattern of this intermediate phase was indexed to a hexagonal $R\bar{3}c$ lattice with lattice parameters $a = 10.65$ nm and $c = 7.53$ nm and the LC state is confirmed by the diffuse WAXS with a maximum at $d = 0.46$ nm (Fig. 4a). The centrosymmetric space group offers a way to construct a reliable ED map with phase choice of 0 and π based on a trial and error approach considering the molecular parameters (see Section S3).

The ED map of the $Hex/R\bar{3}c$ phase shows a double network (Fig. 4c, d). All junctions are three-way with two coordinates at (1; 0; 0.75) and (0; 0.75; 0.25). The two networks show a high similarity between $Ia\bar{3}d$ and $R\bar{3}c$ if viewed from the (111) and

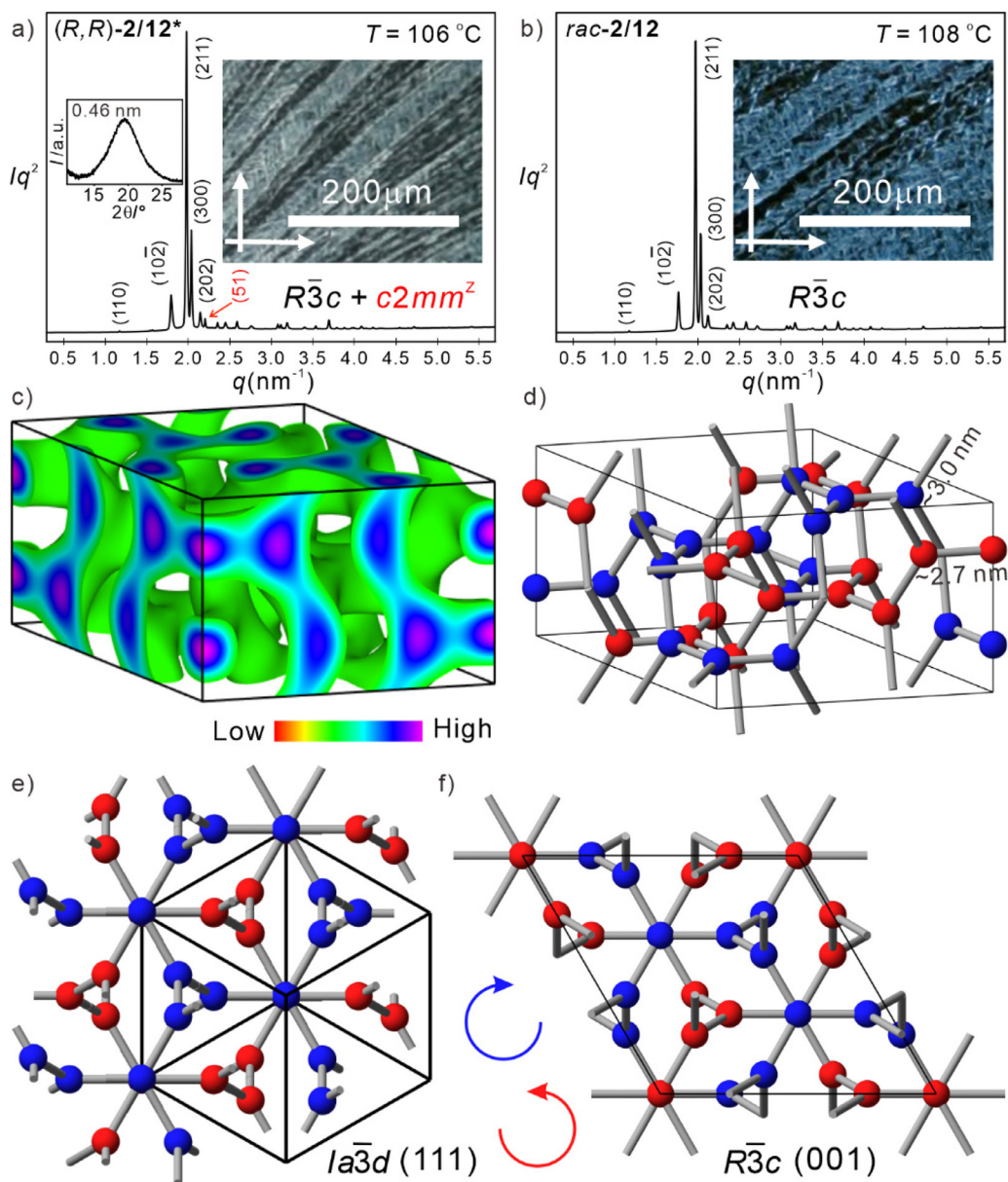


Fig. 4

a, b) SAXS patterns of the Hex/ $R\bar{3}c$ phases with indexation of a) $2/12^*$ at 106 °C (the (51) reflection in red is from the emerging $Col_{rec}^Z/c2mm$ phase, inset: WAXS diffractograms with diffuse scattering maximum at 0.46 nm) and b) $2/12$ at 108 °C; the insets show the textures between crossed polarizers at the same temperatures, c) ED map and d) stick-ball model showing the double network structure; e, f) schemes of e) $Ia\bar{3}d$ along the (111) direction and f) Hex/ $R\bar{3}c$ along the (001) direction; red and blue nodes indicate the networks with opposite handedness. (For interpretation of the references to color in this figure legend, the reader is referred to the web version of this article.)

(001) direction, respectively (Fig. 4e, f). Such similarity is in line with the epitaxial relationships found in many cubic to hexagonal lattice transitions, retaining the $\bar{3}$ symmetry. The lattice parameter a is fixed by the junction position and the aromatic core length, while c is smaller than a_{cub} ($Ia\bar{3}d$) because the dihedral angle between neighboring junction planes deviates from 70.5° in $Ia\bar{3}d$ to ~68° and ~73° in $R\bar{3}c$. Like the $Ia\bar{3}d$ phase, the Hex/ $R\bar{3}c$ phase is also an achiral *meso*-structure, composed of two interwoven networks with opposite handedness (Fig. 4e, f). Unlike $Ia\bar{3}d$ with uniform d_{nodes} , there are two different types of bundles. There are 18 shorter bundles in the ab plane, typically 2.7 nm, and

18 longer ones (3.0 nm) intersecting with the c direction (Table S5). Interestingly, the increase of n_{bundle} during the $Ia\bar{3}d$ to $R\bar{3}c$ transition can be compensated nicely by the average bundle elongation. Upon further cooling, these longer bundles might collapse and this “bond breaking” initiates the reorganization of the molecules at the transition to the $Col_{rec}^Z/c2mm$ phase. Thus, the new non-cubic network phase can be considered as a distorted $Ia\bar{3}d$ lattice with deviating bundle lengths and interjunction twisting angles. It is different from previously reported non-cubic network phases of bolopolyphiles with a larger number of side-chains (Hex/ $P6_3/m$) [58] as well as from those observed in

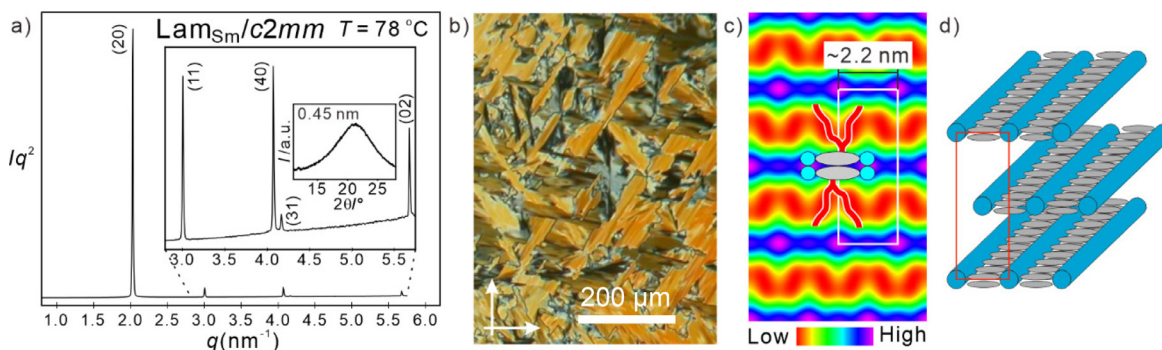


Fig. 5

a) SAXS patterns of the $\text{Lam}_{\text{Sm}}/c2mm$ phase of **2/16*** at 78 °C, inset: WAXS diffractograms with diffuse scattering at 0.45 nm, b) shows the texture of the $\text{Lam}_{\text{Sm}}/c2mm$ phase at 80 °C as observed between crossed polarizers, c) ED map reconstructed from the diffraction pattern, and d) model of the phase.

lyotropic systems (Hex/ $P6_3/mcm$ phases [90–92]), polycatenar LCs [93] and block copolymers [94–97]. To the best of our knowledge, the current Hex/ $R\bar{3}c$ phase is the first experimentally observed LC phase with hexagonal lattice and distorted G minimal surface, which has recently been predicted as a metastable state besides the DG [98,99].

The formation of this phase could be related to the relatively large number of molecules organized in each rod-bundle of the $Ia\bar{3}d$ phase of **2/12***, reaching a critical value of $n_{\text{bundle}} = 15$ on cooling (Table S10). A larger value of about 16 molecules in the Hex/ $R\bar{3}c$ phase (Table S5) requires a pronounced elliptical cross section of the coaxial rod bundles forming the struts connecting the junctions. Simultaneously, the increasing contribution of *all-trans* segments in the alkyl side-chains with lowering temperature provides an increased tendency for parallel chain alignment, leading to a kind of “nematic director field” along a preferred direction (the *c*-axis in $R\bar{3}c$ phase). This in turns provides a certain tendency to reduce the inclination of the rod-bundles with respect to this director field, thus leading to the deformation of the double gyroid and requiring a stretching of the rod-bundles along the *c*-axis. The stretching can be achieved by a deformation of the polar domains from a regular to abuse triangular shape (see Fig. S28b) and by partial overlapping of the glycerols with the outer benzene rings of neighbouring *p*-terphenyls (see Fig. S29) [100]. The transition from the 3D network of the Hex/ $R\bar{3}c$ phase to the $\text{Col}_{\text{rec}}^z/c2mm$ honeycomb is slow, thus leading to a broad DSC feature, especially for the racemic mixture **2/12** (Fig. 2a, b). Again, no significant effect of molecular chirality on the phase structure can be detected. The slight difference in the *c*-parameter of the $R\bar{3}c$ phase of **2/12***, being a bit smaller ($c = 7.53$ nm) than found for the racemate **2/12** ($c = 7.68$ nm) suggests that a slightly denser packing of the uniformly chiral molecules takes place (Fig. 4b, Table S16).

3.1.4 Correlated lamellar phase ($\text{Lam}_{\text{Sm}}/c2mm$)

Upon cooling the longer homologues **2/14*** – **2/18*** a phase transition from the cubic $Ia\bar{3}d$ phase to a birefringent phase with mosaic-like optical textures (see Figs. 5b and S3) is observed, which is different from that of the Hex/ $R\bar{3}c$ and $\text{Col}_{\text{rec}}^z/c2mm$ phases. SAXS investigations of compound **2/16*** at $T = 78$ °C upon cooling show 6 scattering peaks (see Figs 5a, S6b and

S8b and Tables S6, S7) which could be indexed to a centered rectangular lattice with $c2mm$ symmetry and relatively small lattice parameters of $a_{\text{rec}} = 6.18$ nm and $b_{\text{rec}} = 2.22$ nm (see Table 1). The parameter *b* almost stays constant for all compounds whereas *a* increases with growing chain length. Due to the higher intensity of the (20) and (40) layer scatterings in comparison to the (11), (31), (02) and (51) a correlated lamellar phase is likely to be formed (Figs. 5c, d). Within the lamellae the rod-like cores are organized parallel to the layer planes. In the Lam phases the lattice parameter *b* is almost equal to the minimal molecular length ($L_{\text{mol}} = 2.1$ nm) and *a* corresponds to twice the interlayer distance which increases with chain elongation [56]. This structure is confirmed by the ED map (see Fig. 5c) showing alternating modulated layers of high ED (blue/purple = aromatics + glycerols) and undulated layers of low ED (red = alkyl chains). The segregation of the glycerol groups, which form columns of hydrogen bonding network within the layer planes leads to an additional periodicity in these modulated layers (Lam_{Sm}), and the correlation of this periodicity between the layers in an alternating AB mode leads to the centered 2D lattice of this correlated lamellar phase ($\text{Lam}_{\text{Sm}}/c2mm$, Fig. 5d) [56]. One unit cell with a height of 0.45 nm (Fig. 5a) is formed by four mesogens, meaning that each layer has a thickness of about two molecules with back-to-back organized *p*-terphenyl units (see Table S6, S7 and Fig. S25b, c). The gap between the aromatic cores, which is accessible for the alkyl chains, is between 2.0 nm for **2/14*** and 2.4 nm for **2/18*** ($a_{\text{rec}}/2 - 0.9$ nm, the distance of 0.9 nm is the assumed thickness of the aromatic layers formed by pairs of back-to-back arranged molecules). The distance between the *p*-terphenyls and the ends of the side-chains in the most extended conformation (L_{R}) increases from $L_{\text{R}} = 2.1$ nm for **2/14*** to $L_{\text{R}} = 2.6$ nm for **2/18*** if an organization of the chains predominately perpendicular to the layer planes is assumed (Fig. S27a). To achieve an optimal space filling a fully intercalated arrangement of the chains is required. This leads to a significant steric layer coupling, fixing the AB interlayer correlation with $c2mm$ lattice where the bulky side-chains in the middle of the *p*-terphenyls lock into in the gaps around the glycerol groups of the neighbouring layers.

As found for the other LC phases there is no significant difference in optical textures, and lattice parameters if the $\text{Lam}_{\text{Sm}}/c2mm$ phases of the pure enantiomers are compared with

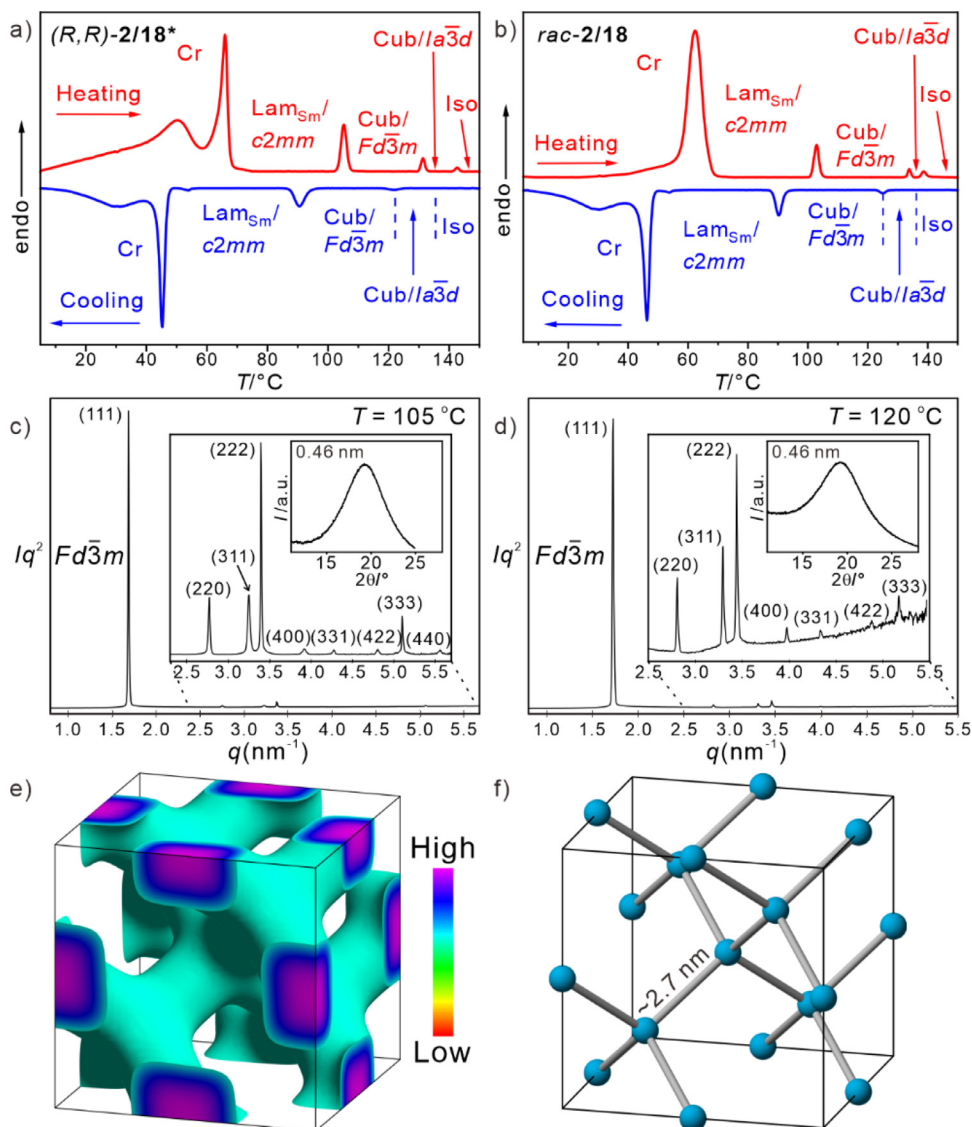


Fig. 6

Cub/ $Fd\bar{3}m$ phase. a, b) DSC traces (10 K min^{-1}) of a) (R,R) -**2/18*** and b) rac -**2/18** (for expanded ranges of the Cub-Cub-Iso transitions, see Fig. S1e,f); c, d) SAXS patterns of c) (R,R) -**2/18*** at $105 \text{ }^\circ\text{C}$ and d) rac -**2/18** at $120 \text{ }^\circ\text{C}$, insets: WAXS diffractograms with diffuse scattering at 0.46 nm ; e) ED map and f) stick-ball model showing the single network structure of the $Fd\bar{3}m$ phase; though the glycerol domains are shown as spheres they actually assume a truncated tetrahedral shape; for NMR spectra of rac -**2/18** and (R,R) -**2/18***, see Figs. S38-S41.

the corresponding mixtures of diastereomers **2/n** (Tables S6, S7 and S17, S18). Larger differences were found for the transition temperatures and associated enthalpies. The reason is that at the transition to 3D ordered crystalline phases and the cubic mesophases, surrounding these Lam phases, kinetic phenomena become important.

The $Lam_{Sm}/c2mm \rightarrow Ia\bar{3}d$ transition temperature decreases upon chain elongation and after transition of the cubic network structure from $Ia\bar{3}d$ to $Fd\bar{3}m$ the $Lam_{Sm}/c2mm$ phase disappears for **2/20*** and **2/20**, which form exclusively the cubic $Fd\bar{3}m$ phase.

3.1.6 Single diamond network phase ($SD = Cub/Fd\bar{3}m$)

The optical isotropic mesophase of the long chain compounds **2/18-2/22** and the corresponding enantiomers **2/18*** and **2/20*** was identified as cubic phase with $Fd\bar{3}m$ space group and single

diamond (SD) network structure (Figs. 6e, f and S9), as analysed in detail for the racemates **2/18-2/22** [61]. In this single network cubic phase the individual rod bundles are interconnected by tetrahedral 4-way instead of the coplanar 3-way junctions in the DG phase, thus leading to a diamond network. The pair **2/18** & **2/18*** is compared in Fig. 6. The distance between each pair of junctions is calculated as $d_{nodes} = (3^{1/2} \cdot a_{cub})/4$ [101] to $\sim 2.76 \text{ nm}$ (Tables S9, S10) and is close to a single molecular length ($L_{mol} = 2.6 \text{ nm}$) considering the substantial size of the glycerol “spheres” at the nodes. In all cases the rod-bundles between the junctions are formed by about 9–10 coaxial aligned molecules in the cross section, and the number decreasing with growing side-chain volume (Table 1). These values are smaller than found in the DG phase, in line with the increase of the coordination number from 3 to 4 which requires thinner bundles to retain the size of

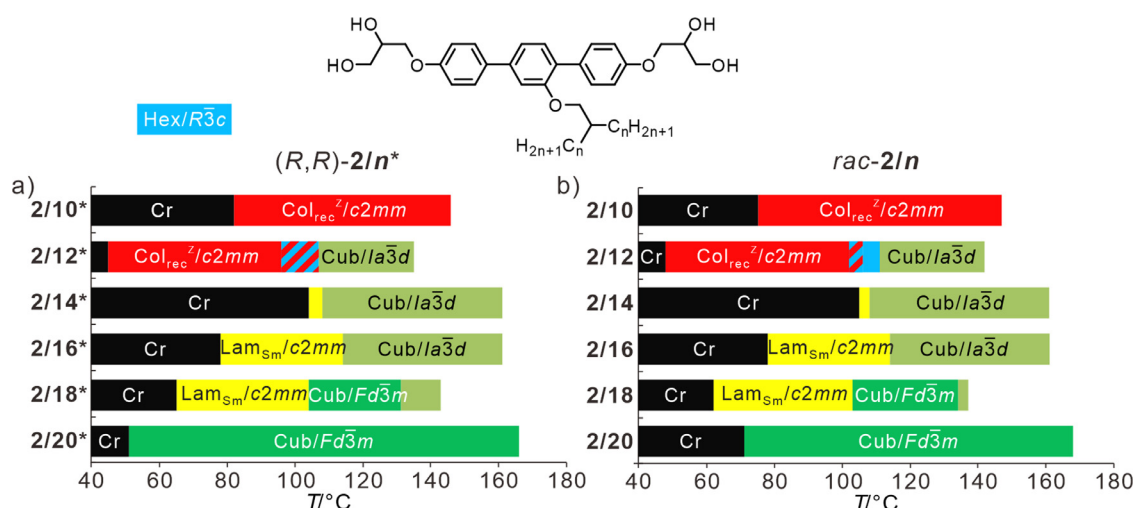


Fig. 7

Comparison of LC phase transitions on heating of a) the (R,R)-enantiomers **2/n*** and b) the racemic mixtures **2/n**, for numerical data and abbreviations see Tables 1 and 2. Note that for **2/12*** and **2/12** data upon cooling are shown to include the Hex/R $\bar{3}c$ phase; the red/blue striped areas indicate the coexistence of Col_{rec}^Z/c2mm and R $\bar{3}c$ in the temperature range of the broad transitions. (For interpretation of the references to color in this figure legend, the reader is referred to the web version of this article.)

the glycerol spheres. The larger density of the struts (number of rod-bundles per constant volume unit) in the diamond network removes the interpenetration, leading to a single network phase.

Compound **2/18*** and its racemic mixture **2/18**, being located at the cross-over from DG to SD combine both cubic phases (Fig. 6a, b). Formation of the DG above the SD could be supported by a higher conformational entropy of the more disordered side-chains in the DG phase [73]. The diamond network itself is achiral and, as expected, no differences could be found between the SD phases formed by the enantiomers and their racemic mixtures, except for deviations due to kinetic effects (hysteresis of phase transitions).

3.1.7 Effects of uniform headgroup chirality on LC self-assembly

The phase sequences and transition temperatures of the (R,R)-enantiomers **2/n*** and the racemic mixtures of diastereomers **2/n** with even numbered $n = 10-20$ are compared in Fig. 7. This shows, that the phase types are identical for all investigated pairs of racemic mixture and pure enantiomer. There is no indication of any induction of new phases or any detectable helical superstructure.

However, in the SAXS patterns in all cases investigated with synchrotron radiation the enantiomers show slightly sharper scattering peaks than found for the racemates (Fig. 8), indicating a larger coherence length of the LR order in the LC phases of the enantiomers and an improved packing of the enantiomerically pure molecules.

The transition temperatures between different LC phases and between the LC phases and the isotropic liquid state (as well as the related transition enthalpies) are in most cases almost identical for enantiomers and mixture of racemates; the deviations are in the range of error of $\pm 1-2$ K (compare Tables 1 and 2) if no kinetic effects are involved. The melting and crystallization temperatures show larger differences in few cases, because different crystalline modifications and different kinetics

of crystallization can be expected for the pure enantiomers and the mixtures of stereoisomers. Even the Ia $\bar{3}d$ phase, representing a meso-structure composed of two enantiomeric networks in the ratio 1:1, is for compounds **2/14** and **2/16** not affected by uniform chirality, which suggests that there is no measurable interaction between molecular chirality and network chirality. However, for compounds located at the transitions from the DG to other modes of LC self-assembly there are larger differences in transition temperatures and phase ranges. One such exceptions is the pair **2/12** & **2/12*** located at the transition from honeycombs (Col_{rec}^Z/c2mm) to networks (Cub/Ia $\bar{3}d$, Hex/R $\bar{3}c$). Here the Ia $\bar{3}d$ range is reduced and the R $\bar{3}c$ \rightarrow Col_{rec}^Z/c2mm transition peak in the DSC cooling traces is much sharper for **2/12***, i.e. this transition is faster for the enantiomer than for the racemic mixture **2/12** (see Fig. 2a, b), as also confirmed by POM studies (Figs. S2 and S14). The reduced Ia $\bar{3}d$ range of **2/12*** could partly be due to kinetic effects and would be in line with a stabilization of the Ia $\bar{3}d$ meso-structure of the racemic mixture (diastereomerism). However, this is reversed for the second exception, provided by the pair **2/18** & **2/18***, which is located at the transition from Cub/Ia $\bar{3}d$ to Cub/Fd $\bar{3}m$. Here the temperature range of the Ia $\bar{3}d$ phase is a bit expanded for the enantiomer **2/18***. This unexpected stabilization of the Ia $\bar{3}d$ meso-structure by uniform molecular chirality would be in line with a denser packing of the enantiomers, leading to a stabilization of the DG with respect to the isotropic liquid state. With other words, the improved packing of the uniformly chiral glycerols leads to a slight strengthening of the H-bonding networks which increases the packing density of the LC phases and the coherence length of their network structure and thus can shift the disintegration of the network to higher temperature. This packing effect can probably suppress opposing chirality effects.

As main conclusion, it appears that for the considered compounds the effect of chirality on the packing density is more important than diastereomeric coupling between the permanent

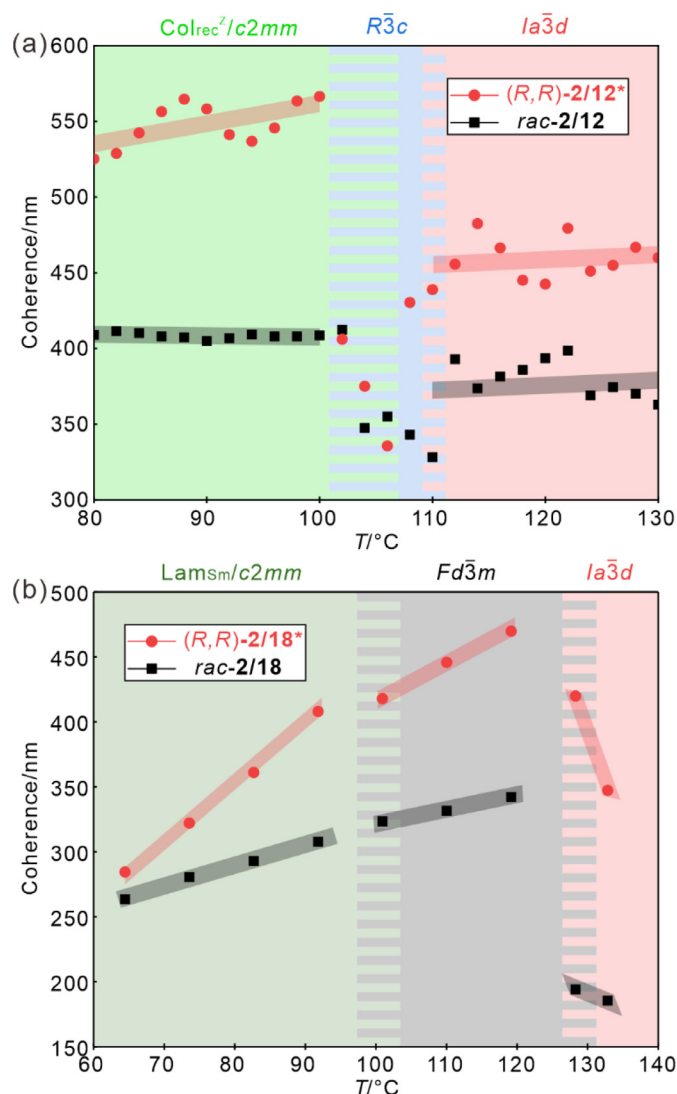


Fig. 8

Comparison between the coherence length a) of enantiomer **2/12*** and racemate **2/12** (note that the $R\bar{3}c$ phase is partially mixed with $Col_{rec}^2/c2mm$ phase for **2/12***; this could lead to an extra decrement of coherence) and b) of enantiomer **2/18*** and racemate **2/18**. The coherence lengths were calculated by $2\pi/\Delta q$, where Δq is the full width at half maximum (FWHM) of the most intense scattering peak; temperature deviation between SAXS and DSC are due to different conditions and heating/cooling rates.

molecular chirality and conformational and superstructural chirality [29,102]. The small effect of head group chirality on mesomorphic self-assembly can be attributed to the dynamic nature of the hydrogen bonding between OH groups in the LC state [103] and the conformational flexibility of the linkages between the OH groups and *p*-terphenyl cores, averaging out any directionality of the hydrogen bondings. The coupling of the *p*-terphenyl cores and stereogenic centres is obviously too weak to bias the helix sense of molecular conformations [102]. The transmission of chiral information between the molecular segments is additionally suppressed by the nano-segregation of the chiral hydrogen bonding glycerols in distinct separate nano-domains (columns and spheres) [37,38]. This isolates the chiral information located in the polar domains which thus

cannot affect the supramolecular self-assembly of other molecular segments, like the *p*-terphenyl rods. In addition, the rods are organized parallel to the IMDSs which disfavours the development of a helical twist, as it would compete with the minimization of the IMDS area. This is not the case for flexible polymers which can easily form chiral networks [104] and for polycatenar rod-like molecules with crowded ends, where the rods are organized perpendicular to the IMDS and show a very strong tendency for the development of a uniform helical twist, thus allowing easy amplification of minor twist induced by permanent or even transient molecular chirality [29,102,105].

In summary, the permanent molecular chirality provided by the polar glycerol groups of bolopolyphiles is obviously incapable to induce new phase structures. As a consequence, racemic mixtures are advantageous over pure enantiomers for the investigation of the complex modes of soft self-assembly of these bolopolyphiles, because often the racemic mixtures have a lower crystallization tendency and sometimes also reduced melting points which increase the phase ranges of the LC phases and the persistence time of metastable LC phases.

3.2 Homologous series **2/n**: full phase sequence depending on side-chain volume

In the following the complete phase sequences of the racemic K-shaped compounds **2/n** depending on temperature and chain length is analysed (Table 2) and compared with the series of T-shaped compounds **1/m** having a linear side-chains with the same chain volume (Fig. 1). The focus is on compounds **2/n** with small side-chain volumes ($n = 4-8$), homologues with odd-numbered $n = 9-15$, and the low temperature phases of the even numbered compounds with $n > 10$ which have not been analysed previously [61,76].

3.2.1 Square and rectangular honeycombs

For the short chain compounds **2/4** – **2/8** X-ray diffraction experiments indicate a square lattice (q ratio of 1: $\sqrt{2}$: 2, $p4mm$) with lattice parameters of $a_{\text{squ}} = 2.63$ nm for **2/4** and 2.64 nm for **2/6** and **2/8** (see Fig. 9c and Tables S12, S13). This is in line with optical investigation between crossed polarizers showing a typical spherulitic textures with dark homeotropic areas of a uniaxial LC phase (Figs. 9a, S11a and S12a). Investigation with a λ -retarder plate indicates negative birefringence as typical for honeycomb LC phases where the main π -conjugation pathway of the *p*-terphenyls (slow axis) is aligned perpendicular to the column long axis (Fig. S12b). For compound **2/8** the X-ray diffraction pattern of a surface aligned sample (X-ray beam parallel to the horizontal surface) additionally confirms the square symmetry (Fig. S17). For all compounds **2/4**–**2/8** the lattice parameter is close to the molecular length in the most stretched conformation (2.6 nm). Altogether, this indicates a square columnar phase in which the *p*-terphenyls form square shaped honeycombs which are filled by the branched side-chains (Figs. 9e, S16a).

The number of molecules per unit cell with a height (in c -direction) of $h = 0.45$ nm decreases with growing chain length from $n_{\text{cell}} = 3.6$ (**2/4**) via 3.2 (**2/6**) to 2.8 (**2/8**), see Table 2. Thus, the honeycomb walls contain on average $n_{\text{wall}} = 1.8$, 1.6, and 1.4 rods, respectively, in each wall with a stratum height of 0.45 nm.

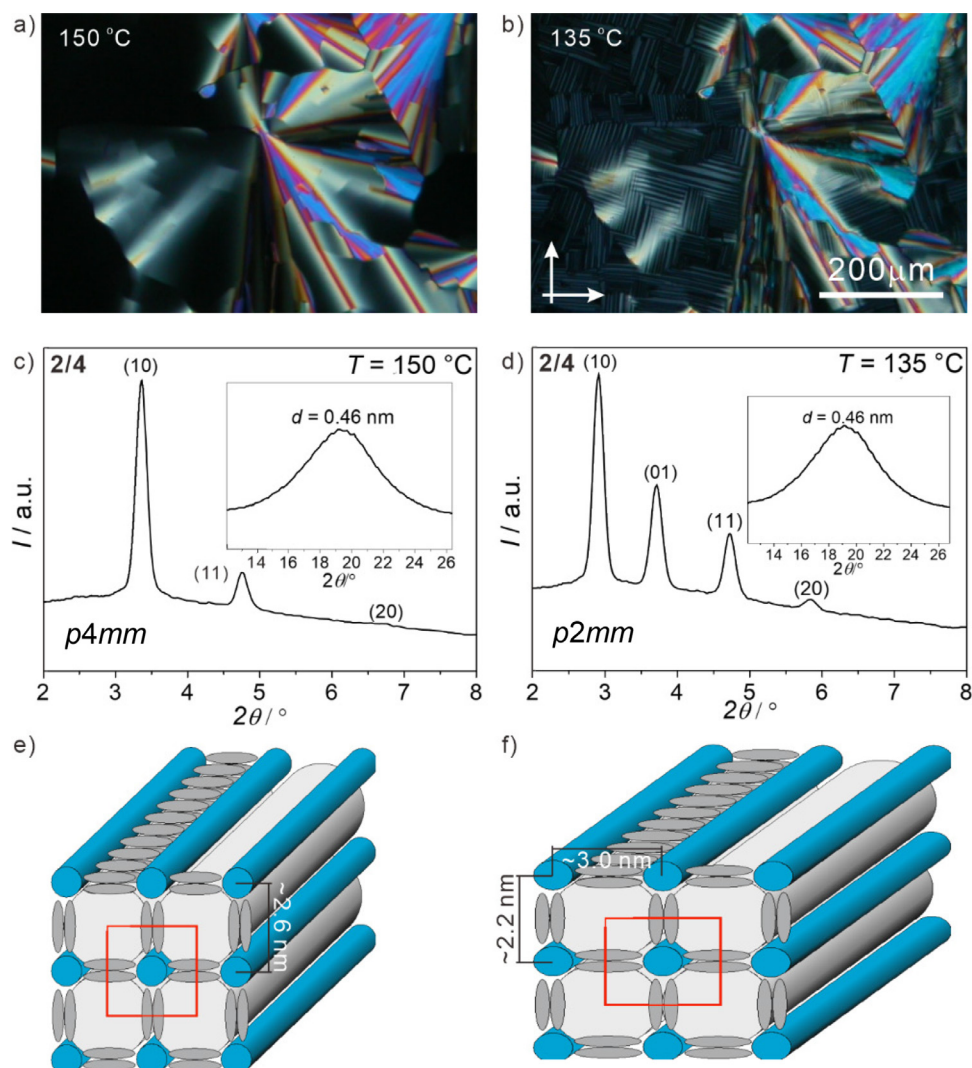


Fig. 9

Square and rectangular honeycomb phases of compound **2/4**; a) texture between crossed polarizers at $T = 150\text{ °C}$ in the $\text{Col}_{\text{squ}}/p4mm$ phase and b) in the $\text{Col}_{\text{rec}}/p2mm$ phase at 135 °C , c) SAXS in the $\text{Col}_{\text{squ}}/p4mm$ phase at $T = 150\text{ °C}$ and d) in the $\text{Col}_{\text{rec}}/p2mm$ phase at 135 °C ; the insets show the WAXS scans, e, f) models of the phase structures; blue – polar columns formed by glycerol groups, gray – terphenyls and white - prismatic cells involving the alkyl side-chains; for XRD and structural data of compounds **2/4**, **2/6** and **2/8** see Tables S12, S13. (For interpretation of the references to color in this figure legend, the reader is referred to the web version of this article.)

For **2/4** with shortest side-chain an almost perfect back-to-back arrangement of two molecules can be assumed, and with growing chain volume the walls become thinner due to an increasing zigzag-like staggering of the *p*-terphenyls along these walls (see Fig. S25b). The total number of C-atoms in the side-chains $m = 2n+2$ (i.e. the side-chain volume) of compound **2/4** with a branched chain ($m = 10$) is the same as for **1/10** in the series of compounds with linear chains (Fig. 1) [49]. Both compounds have the same $\text{Col}_{\text{squ}}/p4mm$ honeycomb phase with almost the same $p4mm$ -Iso transition temperature and number of molecules arranged in the walls ($n_{\text{wall}} = 1.9$ vs. 1.8). In both cases a transition from the square to a rectangular honeycomb is observed on cooling (see below). This means that for this pair of compounds there is almost no effect of the chain branching on the self-assembly.

This is not the case for the two following homologues **2/6** ($m = 14$) and **2/8** ($m = 18$). For these two compounds

the isomeric *n*-alkyl compounds **1/14** and **1/16** with the same side-chain volume form pentagonal (**1/14**) and hexagonal (**1/18**) honeycombs (Fig. 1), while in the series **2/n** the square honeycomb is retained (Table 2). Remarkably, for the series **2/n** the thickness of the honeycomb walls decreases from $n_{\text{wall}} = 1.8$ for **2/4** to 1.4 for **2/8**, while in the pentagonal and hexagonal honeycombs of the related compounds **1/m** with a linear alkyl chain they do not shrink, but slightly expand to become $n_{\text{wall}} = 2.1$ in the pentagonal honeycombs of **1/14** and $n_{\text{wall}} = 2.3$ in the hexagonal honeycombs of **1/18** [49]. This reduction of the honeycomb wall thickness in the series **2/n** can efficiently reduce the number of chains in the polygonal cells and thus allows retaining the square cells for **2/6** and **2/8**, though a transition to a larger cell would be required by the growing volume of the lateral chains. Overall, chain branching stabilizes the smaller square cells over the larger pentagonal and hexagonal cells of the

comparable compounds **1/n**. The main reason is, that the much shorter chains of the branched compounds **2/n** cannot reach the centres of the larger cells without entropically disfavoured chain stretching as it was also discussed in Section 3.1.1 for the $\text{Col}_{\text{rec}}^Z/c2mm$ phase.

Compound **2/8** shows the $\text{Col}_{\text{sq}}/p4mm$ phase exclusively, while compounds **2/4** and **2/6** with shorter side-chains exhibit an additional phase transition with small enthalpy (0.5–0.6 $\text{kJ}\cdot\text{mol}^{-1}$) to another LC phase. At this transition the homeotropic aligned areas in the optical textures disappear and a birefringent pattern of 90° crossed stripes occurs (Figs. 9b and S11b), associated with a change of the SAXS pattern (Fig. 9d). This is typically observed at the transition from square to rectangular columnar phases [49]. The low temperature phase of **2/4** can be indexed as rectangular lattice with $p2mm$ plane group ($\text{Col}_{\text{rec}}/p2mm$) and parameters $a_{\text{rec}} = 3.03$ nm and $b_{\text{rec}} = 2.38$ nm. It is hypothesized, that at this phase transition a slightly increasing contribution of *all-trans* alkyl chain segments to the conformational equilibrium at reduced temperature [100] leads to a preferred parallel alignment of the *all-trans* chain segments parallel to each other and also to the terphenyls in two opposing honeycomb walls, thus providing a “nematic director field” which expands the square cells a bit in direction *a* while shrinking them in direction *b* (see Fig. 9f). This deformation is associated with an elliptical deformation of the polar glycerol columns at the junctions (Fig. S28c-d). It is noted that at this transition the alkyl chains do not crystallize, but remain in a liquid-like fluid state as confirmed by the diffuse WAXS which does not change in width or position at the phase transition (Fig. 9c, d, $d = 0.46$ nm). The temperature of the $\text{Col}_{\text{sq}}/p4mm - \text{Col}_{\text{rec}}/p2mm$ transition decreases with growing chain length from 141 °C for **2/4** to 107 °C for **2/6** and the rectangular phase completely disappears for **2/8** (Table 2). However, this is not driven by the side-chain expansion from **2/4** to **2/8**, because *h* remains almost constant (see Fig. 9c, d) and the unit cell area of the rectangular cells is slightly larger than for the square cells (achieved by a slight increase of the number of molecules in the walls cross-section of the rectangular cells, see Tables. 2 and S13). An alternative explanation is based on restriction of the chain conformation. Because there is a certain preference for the alkyl chains to align parallel to the rod-like units in the rectangular cells, there is a limitation for the chain length. The total length of the lateral chains in their most stretched conformation (between the ends of the two branches, $2n+1$ C-atoms, see Fig. S26a-c) is larger for compounds **2/6** (~1.4 nm, 13 C) compared to **1/11** (~1.3 nm, 11 C), which is the T-shaped molecule with the longest side-chain still capable of forming the $\text{Col}_{\text{rec}}/p2mm$ and $\text{Col}_{\text{sq}}/p4mm$ phases (Fig. 1). For compound **2/8** (17 C) the stretched side-chain length for molecules with H-shaped conformation (~2.0 nm, see Fig. S26b) exceeds the length of the *p*-terphenyl unit (~1.5 nm), and therefore has to remain in a more folded and disordered state. As a result, the square lattice allowing more disordered alkyl chains is retained on cooling.

3.2.2 From honeycombs to networks and layers

The new compounds **2/n** with odd numbered *n* fit well into the sequence of phases observed for the even numbered compounds and no odd-even parity effect [106] can be detected

(Table 2). Increasing the side-chain volume removes the square honeycomb and leads to the highly complex $\text{Col}_{\text{rec}}^Z/c2mm$ phase for compounds with $n = 9-12$. Upon further chain elongation this zeolite-like LC phase is replaced at higher temperature by two network phases with three-way junctions, the monotropic hexagonal $\text{Hex}/R\bar{3}c$ phase and the enantiotropic cubic $\text{Cub}/Ia\bar{3}d$ (DG) phase. For homologs **2/n** with $n > 12$ the $\text{Col}_{\text{rec}}^Z/c2mm$ phase is completely replaced by a lamellar $\text{Lam}_{\text{sm}}/c2mm$ phase at low temperature, while the $\text{Cub}/Ia\bar{3}d$ (DG) phase at higher temperature is retained. Upon further side-chain elongation to $n = 18$ a transition from trigonal 3-way to tetrahedral 4-way junctions takes place in the networks and an additional SD cubic phase with $Fd\bar{3}m$ space group is formed. Associated with the transition from DG ($Ia\bar{3}d$) to SD ($Fd\bar{3}m$) the lamellar $\text{Lam}_{\text{sm}}/c2mm$ phase disappears for $n > 18$ and the SD becomes the exclusively formed LC phase (Fig. 10).

A major contribution to the development of this complex phase sequence comes from packing frustration [101,107] due to the interplay between chain length and chain volume, and the restrictions by the relatively well-defined length of the *p*-terphenyl rods. The dV/dr diagrams [61] compared in Fig. 11, which were calculated with the actual lattice parameter of compounds **2/n** ($n = 6$ to 18, see Section S4) explain nicely the emergence of different phases upon chain elongation. Accordingly, large volumes at short distance *r* support the square, rectangular and $\text{Col}_{\text{rec}}^Z/c2mm$ phases, while the network phases require sufficient space filling at larger distances *r*. The larger effective chain diameter of the branched chains also provides a larger tendency to develop negative IMDS curvature between the polar (core+glycerol) regions and the non-polar aliphatic side-chain regions, additionally supporting the transition from honeycombs with highest positive via $\text{Col}_{\text{rec}}^Z/c2mm$ with smaller positive and Lam with zero curvature to the network phases with negative curvature.

In addition, there is a temperature dependence, leading to two different phase sequences upon elongation of the branched chains; a high temperature sequence $\text{Col}_{\text{sq}}/p4mm \rightarrow \text{Col}_{\text{rec}}^Z/c2mm \rightarrow \text{DG} (Ia\bar{3}d) \rightarrow \text{SD} (Fd\bar{3}m)$, and at low temperatures a sequence $\text{Col}_{\text{rec}}/p2mm \rightarrow \text{Col}_{\text{rec}}^Z/c2mm \rightarrow (\text{Hex}/R\bar{3}c) \rightarrow \text{Lam}_{\text{sm}}/c2mm \rightarrow \text{SD} (Fd\bar{3}m)$ (Fig. 10). This means that the lamellar phase with zero curvature, which is omitted in the high temperature sequence, obviously requires a contribution from side-chain stiffening and the associated parallel chain ordering by the increasing contribution of the *all-trans* alkyl chain segments. This is likely to also contribute to lattice deformations as found for the $\text{Col}_{\text{rec}}/p2mm$ and $\text{Hex}/R\bar{3}c$ phases.

Apart from alkyl chain volume and shape, the valency (coordination number = CN) and shape of the nodes also affects the phase transition among different network phases. For all network phases of compounds **2/n**, there are 33–49 glycerol groups in each node (see Tables S5, S10, and S20). In the DG ($Ia\bar{3}d$) phase the nodes with CN = 3 are flattened into a triangular shape as each node interconnects three identical coplanar rod-bundles [108]. Though the trigonal node shape is far from spherical (which is supposed to minimize their interface area), these networks are divided by a G minimal surface, which

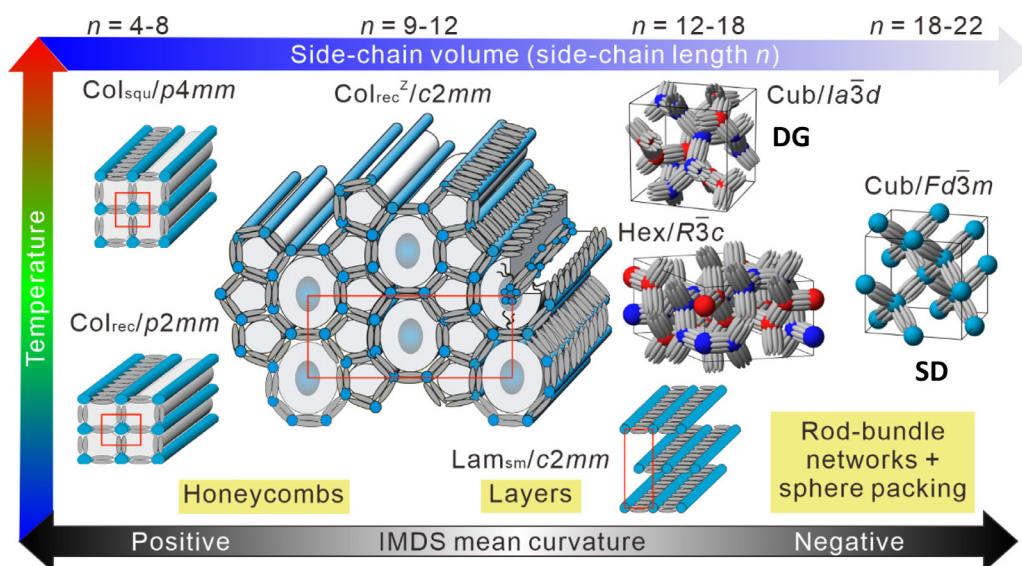


Fig. 10

Overall phase sequence of the K-shaped bolapolyphiles $2/n$ and $2/n^*$ depending on the side-chain length and temperature; Hex/ $R\bar{3}c$ is a distorted version of Cub/ $la\bar{3}d$ phase.

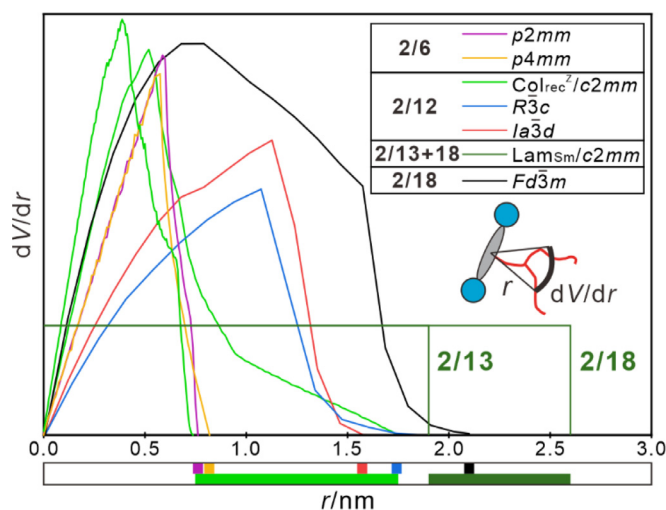


Fig. 11

dV/dr curves of three compounds with all mesophases formed by $2/n$ and $2/n^*$. The bar below exhibits the potential range covered by different phases; for calculations, see Section S4. Most phases are of almost fixed lattice parameters. Only two phases (Col_{rec}²/*c2mm* and Lam_{sm}/*c2mm*) are shown by acceptance regions. For Col_{rec}²/*c2mm*, light green curves represent two extreme situations – the alkyl chains of rod-bundle columns are perpendicular/parallel to the aromatic core (Fig S26c,d). For Lam_{sm}/*c2mm*, dark green curves represent different lattice parameters for $2/13$ and $2/18$, respectively. (For interpretation of the references to color in this figure legend, the reader is referred to the web version of this article.)

becomes distorted in the Hex/ $R\bar{3}c$ phase. The CN of the SD ($Fd\bar{3}m$) phase is 4, being tetrahedral and thus closer to a spherical shape with reduced interfacial area. This increase of valency at almost constant glycerol number also reduces the number of molecules in the rod-bundles and thus provides increased negative IMDS curvature around these bundles, supported by the growing chain

volume. As the strut density per volume unit increases at the G→D transition, the network interpenetration is removed, leading to a double- to single-network transition which provides more space for the side-chains. The single network structure of the SD phase is surprisingly stable with respect to temperature range and side-chain volume, removing all competing LC phases for the long chain compounds $2/20$ and $2/22$. It appears that the diamond structure provides the critical minimum CN for disintegration of double networks into single networks. While for CN = 3 only the DG is spontaneously formed as thermodynamic equilibrium structure, the DD [58,60] and SD [61] cubic phases are both known for CN = 4. By proper molecular design of bolapolyphilic compounds a series of additional new network phases with larger CN was found which all represent single network cubic LC phases, like the single Plumbers Nightmare (SP, $Pm\bar{3}m$, CN = 6) [62], the I-WP ($Im\bar{3}m$, CN = 8) [63] and the A15 network phase ($Pm\bar{3}n$, CN = 12&14) [64]. This sequence of network phases is distinct from the usually recorded sequence DP-DD-DG as known from lyotropic systems [109] and block copolymers [110] formed by flexible amphiphiles. We attribute this to the threefold segregation in the unicontinuous segmented network phases and the restrictions provided by the fixed geometry and distances of the rod-like units [111,112].

It is interesting to note here, that the phase sequences actually observed for the series $2/n^{(*)}$ are a bit different from the sequence Col_{squ} → SP ($Pm\bar{3}m$) → SD ($Fd\bar{3}m$) → DG ($la\bar{3}d$) predicted by coarse grained molecular dynamics simulations for these tethered rods [73]. Though the formation of the SD ($Fd\bar{3}m$) and DG ($la\bar{3}d$) phases has correctly been predicted, the sequence SD ($Fd\bar{3}m$) → DG ($la\bar{3}d$) is opposite, and the Col_{rec}²/*c2mm* honeycomb obviously replaces the predicted SP ($Pm\bar{3}m$) phase. Nevertheless, a Col_{rec}²/*c2mm*-like honeycomb structure has recently been found in simulations using the Mie force field [72], but in this case without the additional columns in the octagons, probably due to the

limitations of the used simulation box in the *c*-direction. On the other hand, the SP ($Pm\bar{3}m$) phase has been experimentally detected for Π -shaped bolopolyphiles having two linear side-by-side arranged chains at the central benzene ring (catechol diethers, see Scheme S1) [62]. It appears that formation of the SP ($Pm\bar{3}m$) phase requires more space filling close to the core unit which is not possible for compounds with a single branched side-chain with some gap between aromatic core and branching point. It is also interesting to note that a hexagonal diamond lattice was predicted by coarse-grained simulation [75], while a hexagonal phase with gyroid network structure was actually found.

4 Summary and conclusions

A unique series of 7 different LC phases was observed for the K-shaped *p*-terphenyl based bolopolyphiles **2/n** with a branched side-chain by simultaneous elongation of both branches and depending on temperature (Fig. 10). All LC phases, with exception of only two ($p2mm$ and $p4mm$), are different from those observed for the isomeric T-shaped bolopolyphiles **1/m** with linear chains (Fig. 1). While honeycombs are dominating in the series of T-shaped compounds **1/m**, network phases become dominating for the K-shaped compounds **2/n**. This is explained by the larger cross-section of the branched chains and that their chain ends have a shorter distance to the *p*-terphenyl core if compared with compounds having the same volume, but a single linear chain. These shorter chains at constant chain volume need to be stretched in order to fill any polygonal cell larger than a square which provides a steric and entropic penalty for the development of the larger prismatic cells [113]. Therefore, the square honeycomb is retained as long as possible and the honeycombs with larger cells are replaced by the complex zeolite-like honeycomb LC formed by pentagons and octagons, with additional strings of coaxial rod-bundles filling the free space in the larger octagons ($Col_{rec}^2/c2mm$).

Further chain elongation favours the rod-bundles and thus leads to a transition to a series of three different network phases, the cubic DG ($Ia\bar{3}d$), a noncubic phase with hexagonal 3D-lattice ($R\bar{3}c$) and a single diamond (SD, $Fd\bar{3}m$) cubic LC phase. All three belong to the new class of unicontinuous network phases [58], characterized by networks having nano-segregated domains at their nodes ("mesoatoms"), interconnected by coaxial rod-bundles ("bonds"). Among them, the new Hex/ $R\bar{3}c$ phase has the same network topology as the DG, but distorted. It is a hexagonal 3D-network with three-way junctions, not being a mesh phase [94], but the first with gyroid-like minimal surface.

The SD, having tetrahedral junctions replaces the DG with trigonal junctions at high side-chain volume. It is the first single network LC phase ever observed and turned out to be surprisingly stable [61]. In the meanwhile, also the single Plumber's nightmare (SP) was discovered [62], while the single gyroid (SG) is still missing in bottom up self-assembled soft matter systems [114,115]. It turned out that besides minimal surfaces and dense packing also the shape of the junctions has a significant influence on tuning the self-assembled structure.

It is also shown that uniform chirality of the glycerol headgroups has no measurable effect on the mesophase structures and does not induce any LR helical superstructures. This is

attributed to the dynamic character of the hydrogen bonding between the glycerols [103] and the conformational flexibility of the glycerol groups, thus becoming less directional and largely decoupled from the molecular cores. The decoupling is further supported by the nano-scale segregation.

Overall, based on the *p*-terphenyl platform with two glycerol end groups, more than 20 new and often highly complex LC mesophases have been discovered to date [43,44,49,50,54,57,61,62,76,82,116,117]. All these new LC phases were achieved only by variation of the volume, length, chemistry, topology, number, position and density of flexible side-chain(s) grafted to a simple *p*-terphenyl platform. These LC structures are considered as highly dynamic soft matter analogues of related solid-state nanoscale structures, such as metal-organic frameworks (MOFs), covalent organic frameworks (COFs) and hydrogen bonded or halogen bonded frameworks (HOFs, XOFs) based on reticular solid-state chemistry [118–125]. It also shows that the network approach, initially developed in structural inorganic chemistry [126,127] is also of relevance for soft matter self-assembly. Moreover, these polyphilic multiblock molecules can alternatively be regarded as monodisperse low molecular mass and high- χ relatives [128] of star-shaped multiblock copolymers (microarm star polymers) [86,114], forming complex morphologies on a smaller length scale than the polymers.

Declaration of competing interest

The authors declare that they have no known competing financial interests or personal relationships that could have appeared to influence the work reported in this paper.

Data availability

Data will be made available on request.

CRediT authorship contribution statement

Silvio Poppe: Writing – original draft, Investigation. **Anne Lehmann:** Investigation. **Matthias Steimecke:** Investigation. **Marko Prehm:** Investigation. **Yangyang Zhao:** Investigation. **Changlong Chen:** Investigation, Data curation. **Yu Cao:** Writing – review & editing, Visualization, Investigation, Data curation. **Feng Liu:** Supervision, Project administration, Funding acquisition. **Carsten Tschierske:** Conceptualization, Writing – review & editing, Supervision, Project administration, Funding acquisition.

Acknowledgements

This work is supported by the Deutsche Forschungsgemeinschaft (DFG, Nr. 436494874-GRK 2670), the National Natural Science Foundation of China (No. 12204369), China Postdoctoral Science Foundation (2022M712551, 2023T160505). The authors thank beamlines BL16B1 at Shanghai Synchrotron Radiation Facility (SSRF) for providing the beam time.

Supplementary materials

Supplementary material associated with this article can be found, in the online version, at doi:10.1016/j.giant.2024.100254.

References

- [1] G.M. Whitesides, B. Grzybowski, Self-assembly at all scales, *Science* 295 (2002) 2418–2421.
- [2] S.I. Stupp, L.C. Palmer, Supramolecular chemistry and self-assembly in organic materials design, *Chem. Mater.* 26 (2013) 507–518.
- [3] J.-M. Lehn, Perspectives in supramolecular chemistry—from molecular recognition towards molecular information processing and self-organization, *Angew. Chem. Int. Ed.* 29 (1990) 1304–1319.
- [4] J.F. Stoddart, *Nat. Chem.* 1 (2009) 14.
- [5] P.J. Collings, J.W. Goodby, *Introduction to Liquid Crystals: Chemistry and Physics*, 2nd ed., CRC Press, Boca Raton, FL, 2019.
- [6] N. Koide (Ed.), *The Liquid Crystal Display Story: 50 Years of Liquid Crystal R&D That Lead The Way to the Future*, Springer, Tokyo, 2014.
- [7] X. Chen, E. Körblova, D. Dong, X. Wei, R. Shao, L. Radzihovsky, M.A. Glaser, J.E. MacLennan, D. Bedrov, D.M. Walba, N.A. Clark, First-principles experimental demonstration of ferroelectricity in a thermotropic nematic liquid crystal: polar domains and striking electro-optics, *Proc. Natl. Acad. Sci. U.S.A.* 117 (2020) 14021–14031.
- [8] J. Li, H. Nishikawa, J. Kougo, J. Zhou, S. Dai, W. Tang, X. Zhao, Y. Hisai, M. Huang, S. Aya, Development of ferroelectric nematic fluids with giant- ϵ dielectricity and nonlinear optical properties, *Sci. Adv.* 7 (2021) eabf5047.
- [9] R.J. Mandle, A new order of liquids: polar order in nematic liquid crystals, *Soft Matter* 18 (2022) 5014–5020.
- [10] E. Cruickshank, P. Rybak, M.M. Majewska, Shona Ramsay, C. Wang, C. Zhu, R. Walker, J.M.D. Storey, C.T. Imrie, E. Gorecka, D. Pociecha, To be or not to be polar: the ferroelectric and antiferroelectric nematic phases, *ACS Omega* 8 (2023) 36562–36568.
- [11] T. Wöhrle, I. Wurzbach, J. Kirres, A. Kostidou, N. Kapernaum, J. Litterscheidt, J.C. Haenle, P. Staffeld, A. Baro, F. Gieselmann, S. Laschat, Discotic liquid crystals, *Chem. Rev.* 116 (2016) 1139–1241.
- [12] K. Borisch, S. Diele, P. Göring, H. Kresse, C. Tschierske, Design of thermotropic liquid crystals with micellar cubic mesophases: amphiphilic N-(2,3-Dihydroxypropyl)benzamides, *Angew. Chem. Int. Ed. Engl.* 36 (1997) 2087–2089.
- [13] K. Borisch, S. Diele, P. Göring, H. Kresse, C. Tschierske, Tailoring thermotropic cubic mesophases: amphiphilic polyhydroxy derivatives, *J. Mater. Chem.* 8 (1998) 529–543.
- [14] B.M. Rosen, C.J. Wilson, D.A. Wilson, M. Peterca, M.R. Imam, V. Percec, Dendron-mediated self-assembly, disassembly, and self-organization of complex systems, *Chem. Rev.* 109 (2009) 6275–6540.
- [15] S. Kutsumizu, Recent progress in the synthesis and structural clarification of thermotropic cubic phases, *Isr. J. Chem.* 52 (2012) 844–853.
- [16] M. Funahashi, Nanostructured liquid-crystalline semiconductors – a new approach to soft matter electronics, *J. Mater. Chem. C* 2 (2014) 7451–7459.
- [17] M. O'Neill, S.M. Kelly, Ordered materials for organic electronics and photonics, *Adv. Mater.* 23 (2011) 566–584.
- [18] M. Lehmann, Phase transitions in complex functional liquid crystals—the entropy effect, *Front. Soft. Matter* 3 (2023) 1089726.
- [19] S. Sergeev, W. Pisula, Y.H. Geerts, Discotic liquid crystals: a new generation of organic semiconductors, *Chem. Soc. Rev.* 36 (2007) 1902–1929.
- [20] M. Kumar, S. Kumar, Liquid crystals in photovoltaics: a new generation of organic photovoltaics, *Polym. J.* 49 (2017) 85–111.
- [21] A.P.H.J. Schenning, E.W. Meijer, Supramolecular electronics; nanowires from self-assembled p-conjugated Systems, *Chem. Commun.* 26 (2005) 3245–3258.
- [22] E. Bukusoglu, M.B. Pantoja, P.C. Mushenheim, X. Wang, N.L. Abbott, Design of responsive and active (Soft) materials using liquid crystals, *Annu. Rev. Chem. Biomol. Eng.* 7 (2016) 163–196.
- [23] E.-K. Fleischmann, R. Zentel, Liquid-crystalline ordering as a concept in materials science: from semiconductors to stimuli-responsive devices, *Angew. Chem. Int. Ed.* 52 (2013) 8810–8827.
- [24] Y. Wang, H. Xu, X. Zhang, Tuning the amphiphilicity of building blocks: controlled self-assembly and disassembly for functional supramolecular materials, *Adv. Mater.* 21 (2009) 2849–2864.
- [25] T. Kato, J. Uchida, T. Ichikawa, T. Sakamoto, Functional liquid crystals towards the next generation of materials, *Angew. Chem. Int. Ed.* 57 (2018) 4355–4371.
- [26] H.K. Bisoyi, Q. Li, Liquid crystals: versatile self-organized smart soft materials, *Chem. Rev.* 122 (2022) 4887–4926.
- [27] A. Yoshizawa, Nanostructured assemblies of liquid-crystalline supermolecules: from display to medicine, *Liqu. Cryst.* 46 (2019) 1950–1972.
- [28] C. Dressel, F. Liu, M. Prehm, X. Zeng, G. Ungar, C. Tschierske, Dynamic mirror-symmetry breaking in bicontinuous cubic phases, *Angew. Chem. Int. Ed.* 53 (2014) 13115–13120.
- [29] C. Tschierske, Mirror symmetry breaking in liquids and liquid crystals, *Liqu. Cryst.* 45 (2018) 2221–2252.
- [30] C. Tschierske, Development of structural complexity by liquid-crystal self-assembly, *Angew. Chem. Int. Ed.* 52 (2013) 8828–8878.
- [31] J.W. Goodby, J.P. Collings, T. Kato, C. Tschierske, H.F. Gleeson, P. Raynes (Eds.), *Handbook of Liquid Crystals*, Wiley-VCH, Weinheim, 2014.
- [32] G. Némethy, Hydrophobic interactions, *Angew. Chem. Int. Ed. Engl.* 6 (1967) 195–206.
- [33] J.N. Israelachvili, *Intermolecular and Surface Forces*, Academic Press, Oxford, 2011.
- [34] J.-M. Lehn, *Supramolecular chemistry: Concepts and Perspectives*, Wiley-VCH, Weinheim, New York, 1995.
- [35] X.-H. Cheng, H.-F. Gao, Hydrogen Bonding for supramolecular liquid crystals, in: *Lecture Notes in Chemistry*, Vol. 88, Springer, Berlin, 2015, pp. 133–183.
- [36] C. Präsang, D.W. Bruce, Halogen-bonded liquid crystals, *Helv. Chim. Acta* 106 (2023) e202300008.
- [37] C. Tschierske, Non-conventional liquid crystals—the importance of micro-segregation for self-organisation, *J. Mater. Chem.* 8 (1998) 1485–1508.
- [38] C. Tschierske, Microsegregation: from basic concepts to complexity in liquid crystal self-assembly, *Isr. J. Chem.* 52 (2012) 935–959.
- [39] J.-F. Sadoc, R. Mosseri, *Geometrical Frustration*, Cambridge University Press, Cambridge, 1999.
- [40] J.-H. Fuhrhop, T. Wang, Bolaamphiphiles, *Chem. Rev.* 104 (2004) 2901–2937.
- [41] C. Tschierske, Liquid crystal engineering – new complex mesophase structures and their relations to polymer morphologies, nanoscale patterning and crystal engineering, *Chem. Sov. Rev.* 36 (2007) 1930–1970.
- [42] C. Tschierske, C. Nürnberg, H. Ebert, B. Glettner, M. Prehm, F. Liu, X.-B. Zeng, G. Ungar, Complex tiling patterns in liquid crystals, *Interface Focus* 2 (2012) 669–680.
- [43] X. Zeng, R. Kieffer, B. Glettner, C. Nürnberg, F. Liu, K. Pelz, M. Prehm, U. Baumeister, H. Hahn, H. Lang, G.A. Gehring, C.H.M. Weber, J.K. Hobbs, C. Tschierske, G. Ungar, Complex multicolor tilings and critical phenomena in tetraphilic liquid crystals, *Science* 331 (2011) 1302–1306.
- [44] F. Liu, R. Kieffer, X. Zeng, K. Pelz, M. Prehm, G. Ungar, Tschierske C, Arrays of giant octagonal and square cylinders by liquid crystalline self-assembly of X-shaped polyphilic molecules, *Nat. Commun.* 3 (2012) 1104.
- [45] M. Poppe, C. Chen, S. Poppe, F. Liu, C. Tschierske, A periodic dodecagonal superlattice by self-assembly of star-shaped molecules in the liquid crystalline state, *Commun. Chem.* 3 (2020) 70.
- [46] M. Kölbl, T. Beyersdorff, X.H. Cheng, C. Tschierske, J. Kain, S. Diele, Design of liquid crystalline block molecules with nonconventional mesophase morphologies: calamitic bolaamphiphiles with lateral alkyl chains, *J. Am. Chem. Soc.* 123 (2001) 6809–6818.
- [47] X. Cheng, M. Prehm, M.K. Das, J. Kain, U. Baumeister, S. Diele, D. Leine, A. Blume, C. Tschierske, Calamitic bolaamphiphiles with (semi)perfluorinated lateral chains: polyphilic block molecules with new liquid crystalline phase structures, *J. Am. Chem. Soc.* 125 (2003) 10977–10996.
- [48] M. Prehm, C. Enders, M.Y. Anzahaee, B. Glettner, U. Baumeister, C. Tschierske, Distinct columnar and lamellar liquid crystalline phases formed by new bolaamphiphiles with linear and branched lateral hydrocarbon chains, *Chem. Eur. J.* 14 (2008) 6352–6368.
- [49] A. Lehmann, A. Scholte, M. Prehm, F. Liu, X. Zeng, G. Ungar, C. Tschierske, Soft rectangular sub-5nm tiling patterns by liquid crystalline self-assembly of T-shaped bolapolyphiles, *Adv. Funct. Mater.* 28 (2018) 1804162.
- [50] A. Lehmann, M. Prehm, C. Chen, F. Liu, X. Zeng, G. Ungar, C. Tschierske, Transition between tangential and co-axial liquid crystalline honeycombs in the self-assembly of Y-shaped bolapolyphiles, *Chem Commun* 54 (2018) 12306–12309.
- [51] A. Saeed, M. Poppe, M.B. Wagner, S. Hauche, C. Anders, Y. Cao, L. Zhang, C. Tschierske, F. Liu, The rhombic honeycomb – a new mode of self-assembly in liquid crystalline soft matter, *Chem. Comm.* 58 (2022) 7054–7057.
- [52] S. Poppe, M. Poppe, H. Ebert, M. Prehm, C. Chen, F. Liu, S. Werner, Bacia K, C. Tschierske, Effects of lateral and terminal chains of X-Shaped bolapolyphiles with oligo(phenylene ethynylene) cores on self-assembly behaviour. Part 1: transition between amphiphilic and polyphilic self-assembly in the bulk, *Polymers* 9 (2017) 471.
- [53] J.S. Lomas, Cooperativity in alkane-1,2- and 1,3-polyols: NMR, QAIM, and IQA study of O_H...OH and C_H...OH bonding interactions, *Magn. Reson. Chem.* 58 (2020) 666–684.
- [54] A. Scholte, S. Hauche, M. Wagner, M. Prehm, S. Poppe, C. Chen, F. Liu, X. Zeng, G. Ungar, C. Tschierske, A self-assembled liquid crystal honeycomb of highly stretched (3-1-1)-hexagons, *Chem. Commun.* 56 (2022) 62–65.
- [55] M. Prehm, F. Liu, U. Baumeister, X. Zeng, G. Ungar, C. Tschierske, The giant-hexagon cylinder network—a liquid-crystalline organization formed by a T-shaped quaternary amphiphile, *Angew. Chem. Int. Ed.* 46 (2007) 7972.
- [56] M. Prehm, C. Enders, X. Mang, X. Zeng, G. Ungar, F. Liu, U. Baumeister, C. Tschierske, Lamellar liquid crystals of in-plane lying rod-like mesogens with designer side-chains: the case of sliding versus locked layers, *Chem. Eur. J.* 24 (2018) 16072–16084.
- [57] S. Poppe, C. Chen, F. Liu, C. Tschierske, A skeletal double gyroid formed by single coaxial bundles of catechol based bolapolyphiles, *Chem. Commun.* 54 (2018) 11196–11199.

- [58] X. Cai, S. Hauche, S. Poppe, Y. Cao, L. Zhang, C. Huang, C. Tschierske, F. Liu, Network phases with multiple junction geometries at the Gyroid-Diamond transition, *J. Am. Chem. Soc.* 145 (2023) 1000–1010.
- [59] F. Liu, M. Prehm, X. Zeng, C. Tschierske, G. Ungar, Skeletal cubic, lamellar, and ribbon phases of bundled thermotropic bolopolyphiles, *J. Am. Chem. Soc.* 136 (2014) 6846–6849.
- [60] X. Zeng, M. Prehm, G. Ungar, C. Tschierske, F. Liu, Formation of a double diamond cubic phase by thermotropic liquid crystalline self-assembly of bundled bolaamphiphiles, *Angew. Chem. Int. Ed.* 55 (2016) 8324–8327.
- [61] X. Zeng, S. Poppe, A. Lehmann, M. Prehm, C. Chen, F. Liu, H. Lu, G. Ungar, C. Tschierske, A self-assembled bicontinuous cubic phase with single-diamond network, *Angew. Chem. Int. Ed.* 58 (2019) 7375–7379.
- [62] S. Poppe, X. Cheng, C. Chen, X. Zeng, R.-B. Zhang, F. Liu, G. Ungar, C. Tschierske, Liquid organic frameworks: the single-network plumbers nightmare” bicontinuous cubic liquid crystal, *J. Am. Chem. Soc.* 142 (2020) 3296–3300.
- [63] C. Chen, M. Poppe, S. Poppe, C. Tschierske, F. Liu, Liquid organic frameworks: a liquid crystalline 8-connected network with body-centered cubic symmetry, *Angew. Chem. Int. Ed.* 59 (2020) 20820–20825.
- [64] C. Chen, M. Poppe, S. Poppe, M. Wagner, C. Tschierske, F. Liu, Tetrahedral liquid crystalline networks: an A15-like Frank Kasper Phase based on rod-packing, *Angew. Chem. Int. Ed.* 61 (2022) e202203447.
- [65] Y. Cao, A. Scholte, M. Prehm, C. Anders, C. Chen, J. Song, L. Zhang, G. He, C. Tschierske, F. Liu, Understanding the role of trapezoids in honeycomb self-assembly—pathways between a columnar liquid quasicrystal and its liquid-crystalline approximants, *Angew. Chem. Int. Ed.* (2023) e202314454.
- [66] R. Zhang, Z. Su, X.-Y. Yan, J. Huang, W. Shan, X.-H. Dong, X. Feng, Z. Lin, S.Z.D. Cheng, Discovery of structural complexity through self-assembly of molecules containing rodlike components, *Chem. Eur. J.* 26 (2020) 6741–6756.
- [67] A.J. Crane, E.J. Martínez-Veracoechea, F.A. Escobedo, E.A. Müller, Molecular dynamics simulation of the mesophase behaviour of a model bolaamphiphilic liquid crystal with a lateral flexible chain, *Soft Matter* 4 (2008) 1820–1829.
- [68] M. Bates, M. Walker, Dissipative particle dynamics simulation of T- and X-shaped polyphilic molecules exhibiting honeycomb columnar phases, *Soft Matter* 5 (2009) 346–353.
- [69] X. Liu, K. Yang, H. Guo, Dissipative particle dynamics simulation of the phase behavior of TShaped ternary amphiphiles possessing rodlike mesogens, *J. Phys. Chem. B* 117 (2013) 9106–9120.
- [70] F. Liu, P. Tang, H. Zhang, Y. Yang, Archimedean tiling patterns self-assembled from XShaped rod–coil copolymers with hydrogen bonds, *Macromolecules* 51 (2018) 7807–7816.
- [71] S.D. Peroukidis, Entropy driven polymorphism in liquids and mesophases consisting of three block amphiphilic molecules, *Soft Matter* 8 (2012) 11062–11071.
- [72] M. Fayaz-Torshizi, E.A. Müller, Coarse-grained molecular dynamics study of the self-assembly of polyphilic bolaamphiphiles using the SAFT- γ Mie force field, *Mol. Syst. Des. Eng.* 6 (2021) 594–608.
- [73] Y. Sun, P. Padmanabhan, M. Misra, F.A. Escobedo, Molecular dynamics simulation of thermotropic bolaamphiphiles with a swallow-tail lateral chain: formation of cubic network phases, *Soft Matter* 13 (2017) 8542–8555.
- [74] T.D. Nguyen, S.C. Glotzer, Reconfigurable assemblies of shape-changing nanorods, *ACS Nano* 4 (2010) 2585–2594.
- [75] Y. Sun, F.A. Escobedo, Coarse-Grained Molecular Simulations of Bolopolyphiles with a Mutident Lateral Chain: Formation and Structural Analysis of Cubic Network Phases, *J. Chem. Theory Comput.* 20 (2024) 1519–1537.
- [76] S. Poppe, A. Lehmann, A. Scholte, M. Prehm, X. Zeng, G. Ungar, C. Tschierske, Zeolite-like liquid crystals, *Nat. Commun.* 6 (2015) 8637.
- [77] J.J. Vallooran, M. Duss, P. Ansoorge, R. Mezzenga, E.M. Landau, Stereochemical purity can induce a new crystalline mesophase in phytantriol lipids, *Langmuir* 36 (2020) 9132–9141.
- [78] H.-S. Kitzerow, C. Bahr (Eds.), *Chirality in Liquid Crystals*, Springer, New York, 2001.
- [79] R.V. Henley, E.E. Turner, The scission of diaryl ethers and related compounds by means of piperidine. Part III. The nitration of 2 : 4-dibromo-2' : 4'-dinitrophenyl ether and of 2 ; 4-dibromophenyl p-toluenesulphonate and benzoate. The chlorination and bromination of m-nitrophenol, *J. Chem. Soc.* (1930) 928–940.
- [80] C. Campbell, D.A. Leigh, I.J. Vitorica-Yrezabal, S.L. Woltering, Construction of boronate ester based single-layered covalent organic frameworks, *Angew. Chem. Int. Ed.* 53 (2014) 13771–13774.
- [81] J.C.Y. Cheng, U. Hacksell, G.D. Daves, Facile Synthesis of 2/-Deoxy-3/-keto- and 2'-deoxypseudouridine derivatives and analogues. Palladium(II)-mediated coupling reactions of furanoid glycols, *J. Org. Chem.* 51 (1986) 3093–30108.
- [82] M. Prehm, F. Liu, X. Zeng, G. Ungar, C. Tschierske, Axial-bundle phases - new modes of 2D, 3D, and helical columnar self-assembly in liquid crystalline phases of bolaamphiphiles with swallow tail lateral chains, *J. Am. Chem. Soc.* 133 (2011) 4906–49016.
- [83] C. Baerlocher, L.B. McCusker, D. Olson, *Atlas of Zeolite Framework Types*, Elsevier, Amsterdam, Boston, 2007 Published on behalf of the Structure Commission of the International Zeolite Association by.
- [84] M. O'Keeffe, B.G. Hyde, Plane nets in crystal chemistry, *Phil. Trans. R. Soc. Lond. A* 295 (1980) 553–618.
- [85] V. Kocman, R.I. Gait, J. Rucklidge, The crystal structure of bikitaite, *Li[AlSi₂O₆]-H₂O*, *Am. Mineral.* 59 (1974) 71–78.
- [86] H. Miyase, Y. Asai, A. Takano, Y. Matsushita, Kaleidoscopic tiling patterns with large unit cells from ABC star-shaped terpolymer/diblock copolymer blends with hydrogen bonding interaction, *Macromolecules* 50 (2017) 979–986.
- [87] Y. Cao, M. Alaasar, L. Zhang, C. Zhu, C. Tschierske, F. Liu, Supramolecular meso-trick: ambidextrous mirror symmetry breaking in a liquid crystalline network with tetragonal symmetry, *J. Am. Chem. Soc.* 144 (2022) 6936–6945.
- [88] G.M. Grason, E.L. Thomas, How does your gyroid grow? A mesoatomic perspective on supramolecular, soft matter network crystals, *Phys. Rev. Mater.* 7 (2023) 045603.
- [89] Y. Liu, T. Liu, X.-Y. Yan, Q.-Y. Guo, J. Wang, R. Zhang, S. Zhang, Z. Su, J. Huang, G.-X. Liu, W. Zhang, W. Zhang, T. Aida, K. Yue, S. Huang, Z.D. Cheng, Mesoatom alloys via self-sorting approach of giant molecules blends, *Giant* 4 (2020) 100031.
- [90] S.T. Hyde, G.E. Schroder, Novel surfactant mesostructural topologies: between lamellae and columnar (hexagonal) forms, *Curr. Opin. Colloid Interface Sci.* 8 (2003) 5–14.
- [91] G.P. Sorenson, A.K. Schmitt, M.K. Mahanthappa, Discovery of a tetracontinuous, aqueous lyotropic network phase with unusual 3D-hexagonal symmetry, *Soft Matter* 10 (2014) 8229–8235.
- [92] Y. Han, D. Zhang, L.L. Chng, J. Sun, L. Zhao, X. Zou, J.Y. Ying, A tri-continuous mesoporous material with a silica pore wall following a hexagonal minimal surface, *Nat. Chem.* 1 (2009) 123–127.
- [93] J. Kain, S. Diele, G. Pelzl, C. Lischka, w. Weissflog, A three-dimensional mesophase with rhombohedral structure formed by double-swallow-tailed compounds, *Liq. Cryst.* 27 (2000) 11–16.
- [94] M. Leaver, A. Fogden, M. Holmes, C. Fairhurst, Structural models of the R3m intermediate mesh phase in nonionic surfactant water mixtures, *Langmuir* 17 (2001) 35–46.
- [95] G.E. Schröder-Turk, T. Varslot, L. de Campo, S.C. Kapfer, W.A. Mickel, Bicontinuous mesophase geometry with hexagonal symmetry, *Langmuir* 27 (2011) 10475–10483.
- [96] A.J. Meuler, M.A. Hillmyer, F.S. Bates, Ordered network mesostructures in block polymer materials, *Macromolecules* 42 (2009) 7221–7250.
- [97] P. Kekicheff, B. Cabane, Between cylinders and bilayers: structures of intermediate mesophases of the SDS/water system, *J. Phys.* 48 (1987) 1571–1583.
- [98] M. Nonomura, T. Ohta, Kinetics of morphological transitions between mesophases, *J. Phys. Chem. B* 13 (2001) 9089–9112.
- [99] M. Imai, A. Saeki, T. Teramoto, A. Kawaguchi, K. Nakaya, T. Kato, K. Ito, Kinetic pathway of lamellar \ gyroid transition: pretransition and transient states, *J. Chem. Phys.* 115 (2001) 10525–10531.
- [100] R. Berardi, F. Spinozzi, C. Zannoni, The conformations of alkyl chains in fluids. A maximum entropy approach, *Chem. Phys. Lett.* 260 (1996) 633–638.
- [101] P.M. Duesing, R.H. Templer, J.M. Seddon, Quantifying packing frustration energy in inverse lyotropic mesophases, *Langmuir* 13 (1997) 351–359.
- [102] C. Tschierske, G. Ungar, Mirror symmetry breaking by chirality synchronisation in liquids and liquid crystals of achiral molecules, *ChemPhysChem* 17 (2016) 9–26.
- [103] G.G. Siegel, P.L. Huyskens, The mobile order created by hydrogen bonds in liquids, in: P.L. Huyskens, W.A.P. Luck, T. Zeegers-Huyskens (Eds.), *Intermolecular Forces*, Springer-Verlag, Berlin, 1991, pp. 387–395.
- [104] K.-C. Yang, A. Reddy, H.-W. Tsai, W. Zhao, G.M. Grason, R.-M. Ho, Breaking mirror symmetry of double gyroids via self-assembly of chiral block copolymers, *ACS Macro Lett* 11 (2022) 930–934.
- [105] H. Ocak, B. Bilgin-Eran, M. Prehm, S. Schymura, J.P.F. Lagerwall, C. Tschierske, Effects of chain branching and chirality on liquid crystalline phases of bent-core molecules: blue phases, de Vries transitions and switching of diastereomeric states, *Soft Matter* 7 (2011) 8266–8280.
- [106] A. Jakli, Odd-even effects in liquid crystals, *Liqu. Cryst.* 49 (2021) 1010–1019.
- [107] C.V. Kulkarni, Calculating the ‘chain splay’ of amphiphilic molecules: towards quantifying the molecular shapes, *Chem. Phys. Lipids* 218 (2019) 16–21.
- [108] Y. Nakazawa, Y. Yamamura, S. Kutsumizu, K. Saito, Molecular mechanism responsible for reentrance to Ia3d gyroid phase in cubic mesogen BABH(n), *J. Phys. Soc. Jpn.* 81 (2012) 094601.
- [109] C.V. Kulkarni, T.-Y. Tang, A.M. Seddon, J.M. Seddon, O. Cesa, R.H. Templer, Engineering bicontinuous cubic structures at the nanoscale—the role of chain Splay, *Soft Matter* 6 (2010) 3191–3194.
- [110] C.-Y. Chang, G.-M. Manesi, C.-Y. Yang, Y.-C. Hung, K.-C. Yang, P.-T. Chiu, A. Avgeropoulos, R.-M. Ho, Mesoscale networks and corresponding transitions from self-assembly of block copolymers, *Proc. Natl. Acad. Sci. U.S.A.* 118 (2021) e2022275118.

- [111] J.-H. Ryu, M. Lee, Liquid Crystalline Assembly of rod-coil Molecules, *Struct. Bond.* 128 (2008) 63–98.
- [112] W. Li, Y. Kim, M. Lee, Intelligent supramolecular assembly of aromatic block molecules in aqueous solution, *Nanoscale* 5 (2013) 7711–7723.
- [113] M.A. Winnik, D. Rigby, R.E.T. Stepto, B. Lemaire, An evaluation of rotational isomeric state model calculations of hydrocarbon chains, with and without excluded volume, *Macromolecules* 13 (1980) 699–704.
- [114] L. Li, Q. Dong, W. Li, Stabilize various novel network structures via the alternate arrangement of A/C domains in close contact by tailoring ABC miktoarm star architectures, *Macromolecules* 57 (2023) 409–419.
- [115] P. Chen, M.K. Mahanthappa, K.D. Dorfman, Stability of cubic single network phases in diblock copolymer melts, *J. Polym. Sci.* 60 (2022) 2543–2552.
- [116] R. Kieffer, M. Prehm, B. Glettner, K. Pelz, U. Baumeister, F. Liu, X. Zeng, G. Ungar, C. Tschierske, X-Shaped polypholics: liquid crystal honeycombs with single-molecule walls, *Chem. Commun.* 44 (2008) 3861–3863.
- [117] C. Chen, R. Kieffer, H. Ebert, M. Prehm, R.B. Zhang, X. Zeng, F. Liu, G. Ungar, Carsten Tschierske, Chirality induction through nano-phase separation: alternating network gyroid phase by thermotropic self-assembly of X-shaped bolopolyphiles, *Angew. Chem. Int. Ed.* 59 (2020) 2725–2729.
- [118] O.M. Yaghi, M. O’Keeffe, N.W. Ockwig, H.K. Chae, M. Eddaoudi, J. Kim, Reticular synthesis and the design of new materials, *Nature* 423 (2023) 705–714.
- [119] O.M. Yaghi, G. Li, H. Li, Selective binding and removal of guests in a microporous metal–organic framework, *Nature* 378 (1995) 703–706.
- [120] A.P. Cote, A.I. Benin, N.W. Ockwig, M. O’Keeffe, A.J. Matzger, O.M. Yaghi, Porous, Crystalline, Covalent Organic Frameworks, *Science* 310 (2005) 1166–1170.
- [121] P.J. Waller, F. Gandara, O.M. Yaghi, Covalent organic frameworks: design principles, synthetic strategies, and diverse applications, *Acc. Chem. Res.* 48 (2015) 3053–3063.
- [122] H.R. Abuzeid, A.F.M. El-Mahdy, S.-W. Kuo, Covalent organic frameworks: Design principles, synthetic strategies, and diverse applications, *Giant* 6 (2021) 100054.
- [123] I. Hisaki, C. Xin, K. Takahashi, T. Nakamura, Designing hydrogen-bonded organic frameworks (HOFs) with permanent porosity, *Angew. Chem. Int. Ed.* 58 (2019) 11160–11170.
- [124] R.-B. Lin, Y. He, P. Ki, H. Wang, W. Zhou, B. Chen, Multifunktional porous hydrogen-bonded organic frameworks, *Chem. Soc. Rev.* 48 (2019) 1362–1389.
- [125] N. Xia, J. Han, F. Xie, G. Gong, L. Wang, J. Wang, S. Chen, Construction of halogen-bonded organic frameworks (XOFs) as novel efficient iodinating agents, *ACS Appl. Mater. Interf.* 14 (2022) 43621–43627.
- [126] A.F. Wells, *Three-Dimensional Nets and Polyhedra*, Wiley, New York, 1977.
- [127] M. O’Keeffe, B.G. Hyde, *Crystal Structures – I. Patterns and Symmetry*, Mineralogical Society of America, Washington, DC, 1996.
- [128] C. Sinturel, F.S. Bates, M.A. Hillmyer, High χ –low N block polymers: how far can we go? *ACS Macro Lett.* 4 (2015) 1044–1050.